Manufacturing Processes for the Development of Unmanned Vehicles

João Miguel Eira Machado

Dissertação de Mestrado

Orientador na FEUP: Prof. Dr. António Torres Marques

Mestrado Integrado em Engenharia Mecânica

Setembro 2016

Processos de Fabrico para desenvolvimento de Veículos Autónomos não Tripulados

Resumo

No âmbito do fabrico de materiais compósitos, nomeadamente na família de processos de *Liquid Composite Moulding* (LCM), a permeabilidade é uma propriedade do meio composto por fibras de reforço. A previsão dos valores de permeabilidade é muito importante para a otimização do processo de fabrico, assim como a possível eliminação de defeitos nas peças fabricadas.

Partindo de uma abordagem com base em elementos de volume representativo de natureza estocástica, valores de permeabilidade longitudinal são derivados a partir de meios fibrosos unidirecionais, gerados aleatoriamente, para diferentes valores de volume de fibra. A análise dos resultados obtidos sugere que a permeabilidade longitudinal segue um modelo de distribuição normal.

Parâmetros de modelos analíticos para previsão de permeabilidade em função da fração volúmica de fibra do meio, foram revistos para uma gama de porosidades de 22% a 50%, tendo como base os resultados obtidos. Desenvolveu-se assim uma equação para cada parâmetro, que descreve o valor numérico deste em função da fração volúmica de fibra do meio.

Finalmente, uma análise ponto a ponto foi conduzida ao longo do comprimento do volume representativo. Os resultados obtidos sugerem que para o caso de simulações numéricas tridimensionais, o quociente entre a largura (ou altura) do volume representativo e o seu comprimento, é um parâmetro muito importante para evitar potenciais erros de resultados.

Manufacturing Processes for the Development of Unmanned Vehicles

Abstract

In the scope of composite materials processing, namely in Liquid Composite Moulding (LCM), permeability is a property of the medium composed by reinforcement fibres. The prediction of permeability is paramount to process optimization and possible elimination of defects in manufactured parts.

By applying a representative volume element approach with stochasticity, permeability is derived from randomly generated porous media at different values of fibre volume fraction, for the case of longitudinal flow in a unidirectional ply. Analysis of the obtained results suggests that permeability follows indeed a normal distribution model.

Also, parameters from models that predict permeability as a function of fibre volume fraction of the medium, are revisited for a porosity range of 22% to 50%, in light of the previous results. An equation was developed for each parameter, describing it as a function of the fibre volume fraction of the medium.

Finally, a point-by-point analysis of permeability is done along the RVE length, whose results suggest that for the case of 3D CFD simulations, the aspect ratio of the RVE is a very important parameter, in order to avoid over-predictions in permeability results.

Acknowledgments

Gostaria de dedicar este trabalho aos meus pais, pelo seu apoio e dedicação incondicional ao longo de toda a minha vida; aos meus irmãos, tios e avós por todo o apoio que também me têm dado desde sempre.

Queria também agradecer aos meus amigos, por me conseguirem animar, mesmo nos momentos mais cansativos.

Finalmente, queria agradecer à Rita por todo o seu apoio e carinho.

I would like to dedicate this thesis to my parents, for their unconditional dedication and support, along my entire life; to my brothers, uncles and grandparents for the support they have also been given.

I also would like to thank my friends, for being capable of cheering me up, even in the most strenuous moments.

Finally, I would like to thank Rita, for all her support and affection.

Also, I would like to thank my co-supervisor, Dr. Nuno Correia, for his giving me the best conditions to work at INEGI and also for purposing such a challenging thematic, to develop my thesis.

To my supervisor, Prof. Dr. Torres Marques, for being always available to help, whenever I encountered a problem.

To Profª. Drª. Teresa Martins, for her precious help in conducting the statistical study.

To Dr. Alexandre Afonso, for his help and advice during the development of this thesis; by always being available to help, even if from an email.

To Luís Varandas, for helping me when I was having trouble on the programming task.

Lastly, a special thanks to Masoud Bodaghi, for his priceless help and encouragement during the development of this thesis. For the long talks, sometimes followed by a cup of coffee, which helped to consolidate all the knowledge, as well as prevent me from overthinking.

Contents

List of Figures

List of Tables

1 Introduction

1.1 Background

Composite materials have been used in aviation since its beginning. The high strength to weight ratio and stiffness inherent to this type of materials makes them a preferable choice over traditional metallic alloys, since aviation strives for low weight structures. Indeed, the increasing incorporation of this type of materials in aircraft structures has led to serious performance improvements in fuel consumption and maintenance costs, also due to their bigger corrosion and fatigue resistance.

Just like in manned aircraft, in unmanned aerial vehicles (UAVs) weight reduction is paramount in order to guarantee fuel economy, therefore extending its flight range and payload capacity.

The evolution of the composite manufacturing processes has led to significant improvements in component design flexibility and reliability, thus allowing the creation of better structures for aviation. However, since the optimization of manufacturing processes is usually based on CAE software, the correct input of the material properties is paramount in order to have accurate results.

In the case of LCM, permeability is a property of the fibre preform that reflects the ease that a fluid flow has to penetrate a given porous medium. Along with the resin fluid properties and injection pressure or flow rate, permeability is a very important input on mould filling software for LCM, since without this property it's impossible to predict mould filling times, also as possible formation of defects (Šimáček and Advani 2004).

This determination of permeability in fibre preforms is done experimentally. However, results are still dominated by a great uncertainty, since the experimental setup conditions are very difficult to control and reproduce. Therefore, there's an effort towards the creation of models capable of describing permeability as function of fibre volume fraction with relevant accuracy. However, the modelling of a realistic system is a very complex task, due to the large spectrum of variables involved, even if analysed at only one scale.

In fact, due to the lack of computational power existent nowadays, it's impossible to model an entire fibre preform and account for all the complex interactions between the fluid resin and the fibres of the preform. Hence, another approach is necessary. Moreover, phases of particles and fluids are usually coupled, establishing interactions along different length scales (Zhu *et al.* 2008). The understanding of the microscopic mechanisms that rule the particle-fluid interactions is therefore paramount, since the macroscopic behaviour of a particulate matter is a reflex of the microscopic behaviour (Zhu *et al.* 2007).

Since permeability is a result from the interactions between a solid phase (fibres) and a fluid phase (resin), it is necessary to have a comprehension of the different factors that govern permeability, at the different length scales.

The study of permeability was also done at minor length scales, where the meso-level (10^{-3} m) corresponds to the analysis of the effect of the textile variations in the resin flow around the fibre bundles, by an unit cell approach (Endruweit *et al.* 2015; Wong and Long 2006). However, this method relies on the averaging of the fibre bundle properties, meaning that a more profound knowledge should already be established for the micro-scale (10^{-6} m).

Despite that, the study of permeability at the micro-scale has been done mainly considering ideal situations. In fact, still a lot of work has to be done in order to identify the main causes of variability in permeability inside the fibre yarns, as well as correctly quantify their effect in order to develop more accurate models.

Finally, it's important to mention that the study of permeability at the meso and micro-scales has been facilitated by the recent developments in computational techniques, since experimental verification is rather difficult or impossible, due to the very small length scales.

1.2 Problem Statement

Since permeability is tightly linked to the porous medium geometry, its variability is a reflex of the variability present in the geometry of the porous medium.

However, in the case of fibre yarns, there are several factors that cause variability in their geometry, e.g. the fibre radius, displacement of the fibres, waviness and misalignment of the fibres.

In order to develop accurate models for permeability, it is therefore necessary to quantify the weight that each one of this factors has on variability of permeability, as well as the potential increase or decrease in permeability magnitude.

1.3 Objectives

The actual study of this thesis focuses on two parts:

The first one is to understand how the random fibre displacement inside a yarn, affects longitudinal permeability, in variability and magnitude. Also, a stochastic model for longitudinal permeability is suggested, based only on the random fibre displacement. This objective is achieved by conducting a series of CFD analysis on representative volume elements with random fibre distribution, on a Monte Carlo method approach. Finally, based on the numerical results, a correction for non-dimensional factors, on porosity-permeability models is also proposed.

The second part of this study focuses on analysing permeability in a point-by-point basis, along the porous media length, since permeability is determined by volume-averaging the Navier-Stokes equation. This study aims for a more profound insight about how permeability behaves inside the porous medium.

1.4 Thesis Layout

This thesis is organized in several chapters, in order to facilitate the reader's understanding of the topics discussed.

Chapter 2 presents a state of the art of several topics.

Firstly, review of the importance of composite materials in the aviation sector is intended to be given, followed by a review of the manufacturing processes that are currently being employed by the industry, for long-fibre reinforced composite materials.

Finally, the last part of the chapter is intended to give a more profound insight about permeability and its importance for composite materials processing, namely LCM.

Chapter 3 is intended to give an explanation about the methods of generation of representative volume elements, as well as the character of the numerical analysis.

Also, an explanation is given about the script responsible to automate the tasks of generating the representative volume elements and conduct the numerical simulations.

Chapter 4 is dedicated to present the results obtained in the numerical simulations, as well as discuss the main conclusions that could be taken, as well as eventually compare the obtained results, with results from previous studies.

Chapter 5 provides the main conclusions regarding the work that was carried out.

Chapter 6 presents some ideas for future works to be carried out.

2 State of the Art

2.1 Composites and aviation

Aerospace companies have been increasingly adopting composite materials in aircraft structures over traditional materials, both for civil and military applications. This was done primarily at small non-structural components. Over the time, not only the number of composite parts has increased, but also the application of these materials has acquired a structural character.

In civil applications, Hinrichsen and Bautista (2001) report that Airbus has increasingly used composite components over traditional metallic alloys, over the last 40 years.

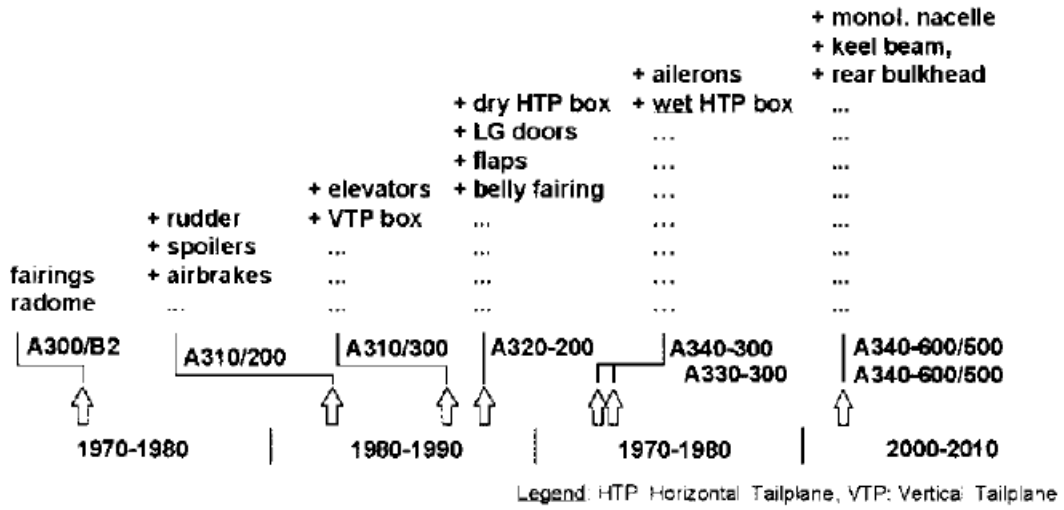

Figure 2.1 - Evolution of composite material applications at Airbus (Hinrichsen and Bautista 2001)

Also, Boeing increased its incorporation of composite materials in the new airliner 787, up to 50% by weight. This is an increase from 12% in the Boeing 777 (Lu 2010).

At the military level, efforts have also been done in order to incorporate these materials over metallic alloys. The Boeing/Northop Grumman F-18 fighter aircraft is a good example of an aircraft where composite materials have been extensively used for performance purposes. Also, in military applications, composite materials have been used in order to reduce radar signature, in stealth designed aircrafts, such as the Northop Grumman B-2 and the Lockheed Martin F-117 stealth bombers. The F-22 fighter is the first aircraft for both military and civilian to incorporate composite parts on the primary structure, fabricated by Resin Transfer Moulding (Mortensen 2007).

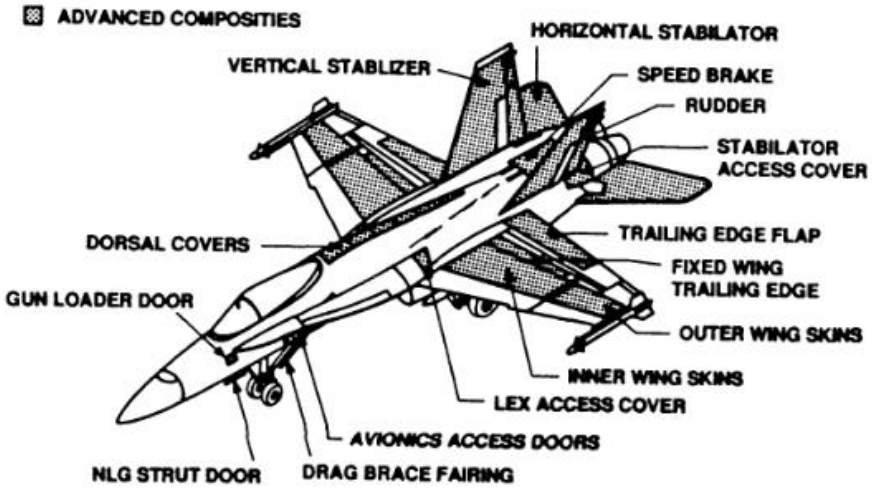

Figure 2.2 - – F-18 C/D Composite Materials Usage (Jones 1999)

However, composite materials cannot be seen only as a way of reducing aircraft weight. As Jones (1998) points out, when composite materials are used over traditional metallic alloys, also the number of parts on the aircraft decreases due to the design flexibility these materials allow. Finally, this reduction in the number of parts has a huge implication in maintenance necessary to keep the airplane flying, measured in maintenance man hours per flight hour.

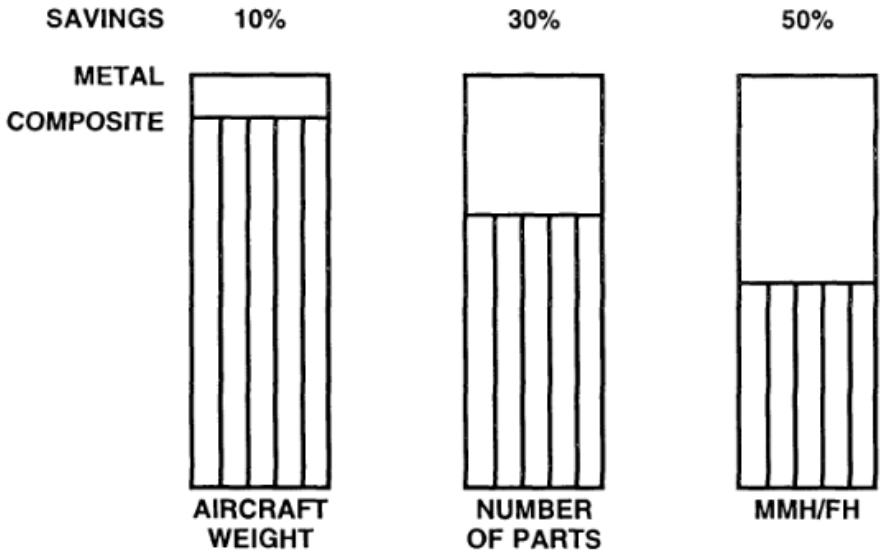

Figure 2.3 - Typical savings in Second-Generation Part-Composite Aircraft (Jones 1999)

So, composite materials impact cannot only be measured by weight reduction on aircraft structures, but a combination of raw materials cost, manufacturing costs, management and warehousing system costs and maintenance costs as a function of the aircraft lifetime, have to be necessarily accounted for.

A review of the composite technologies employed on UAVs is rather difficult because of the poorly documented available information, as the major technological breakthroughs in this area are used for military applications.

2.2 Composite manufacturing processes

When dealing with composite material manufacturing, the manufacturing procedure has a significant impact on the final characteristics of the parts. Be it in mechanical properties, geometry or on cost. A correct choice of the manufacturing route, is therefore very important to maximize part performance and minimize costs.

2.2.1 Autoclave Processing

Autoclave processing is fundamental in aerospace composite manufacturing due to its ability in creating parts with high fibre volume fraction and very low void fraction. This is the main reason why this process is so widely used in this industry. However, due to high energy consumption, parts made by this process are very expensive and, consequently, have significant environmental drawbacks. Also, this manufacturing process isn't capable of high rates of production, which makes it unsuitable for many applications. Part size is also a constraint, because dimensions are limited by autoclave size (Balasubramanian 2014; Hollaway 1994).

Due to all those constraints, out of autoclave processes started to gain a rising importance. Nowadays some out of autoclave processes, e.g. HP-RTM, which will be presented in the next section, can rival autoclave processing, by being capable to create parts with similar fibre volume fraction and void fraction. Also, these processes have additional advantages like the capability to higher production rates and better surface finish.

Figure 2.4 compares different processes that can be used in order to place the reinforcement fabrics in the desired orientation and stack sequence, before autoclave processing.

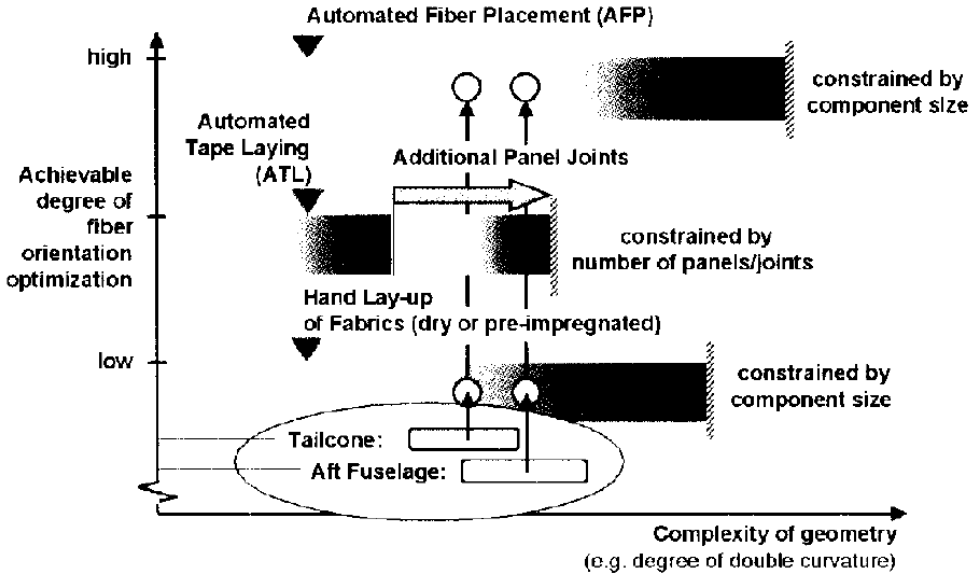

Figure 2.4 - Main parameters for selection of manufacturing process for fuselage panels of A380 (Hinrichsen and Bautista 2001)

2.2.2 Out of Autoclave processing

2.2.2.1 Open Mould Processes

This class includes all the processes that use a single faced mould and therefore expose the fibres and resin to the atmosphere.

Ideally suited for low volume production, hand lay-up is a labour intensive manufacturing process that is very dependent on skilled labour. However, this process is still widely used due to its high flexibility and no need of high capital investment. Indeed, this process is capable of producing large parts with little tooling costs (Campbell 2004; Hollaway 1994; Balasubramanian 2014).

Filament winding is also an open mould process, capable of producing revolution geometries. Despite this limitation, this process is capable of producing parts with excellent mechanical properties and is capable of achieving high production rates. However, as well as in hand lay-up, only one surface of the component gets a smooth finish. In order to achieve a smooth surface finish on both surfaces, additional steps must be taken in these manufacturing processes.

Despite their inherent advantages, open moulding processes have a concerning problem. In fact, because of the resin exposure to the atmosphere when curing, there is a release of styrene to the atmosphere, which is hazardous to health as well as to the environment. According to (Nixon 2000) although composite manufacturing is responsible for only five percent of the overall production of styrene, it's the only industry that exposes its work force to considerable levels of volatile organic compounds (VOC), for which health and safety regulations are getting stricter each year.

2.2.2.2 Closed Mould Processes

One calls a closed mould process when there are two counter moulds, which are joined or clamped. After the mould closure, there is a resin injection into the mould cavity. The female mould can be either rigid or flexible. It is flexible when a foil or silicon bag is used instead of a rigid FRP or metallic female mould.

The possibility of partial or complete automation of this kind of processes and smaller resin cure times, make the manufacturing cycle times of these processes smaller than the ones expected with open mould. In fact, closed mould processes are suitable for medium to high volume production rates, according to automotive industry standards.

Table 2.1 - Automotive volume definition (Rudd *et al.* 1997)

Volume	**Definition**
Low Volume	<10 000 parts per year
Medium Volume	10 000 – 100 000 parts per year
High Volume	>100 000 parts per year

Because in closed mould processes there isn't the problem of the exposure of the resin to atmosphere, this type of processes is therefore more environmentally friendly.

2.2.3 Liquid Composite Moulding (LCM)

Liquid composite moulding or LCM, is a special group of closed mould manufacturing processes that is part of the out of autoclave family of candidates.

LCM can be described generically as a closed mould operation, where a fibre preform is placed in the mould prior to its closure, to be latter impregnated in liquid thermosetting resin. When the resin is cured, the mould is then opened and the component is extracted.

This approach takes the advantages of closed mould processes, allied to a controllable fibre orientation because of the usage of fibre preforms.

As one can expect, depending on the capital investment and with the introduction of automation, these manufacturing processes are capable of medium to high production rates according to the automotive volume definition (Rudd *et al.* 1997). Also, they're capable of manufacturing high performance parts (structural components), due to the allowance of high fibre volume fractions and the potential to incorporate fibres in the necessary orientations to meet structural requirements.

Among others, the most widely used LCM processes in their generic form are Resin Transfer Moulding (RTM), Vacuum Infusion VI, also known as Vacuum Assisted Resin Transfer Moulding (VARTM) and Structural Reaction Injection Moulding (SRIM).

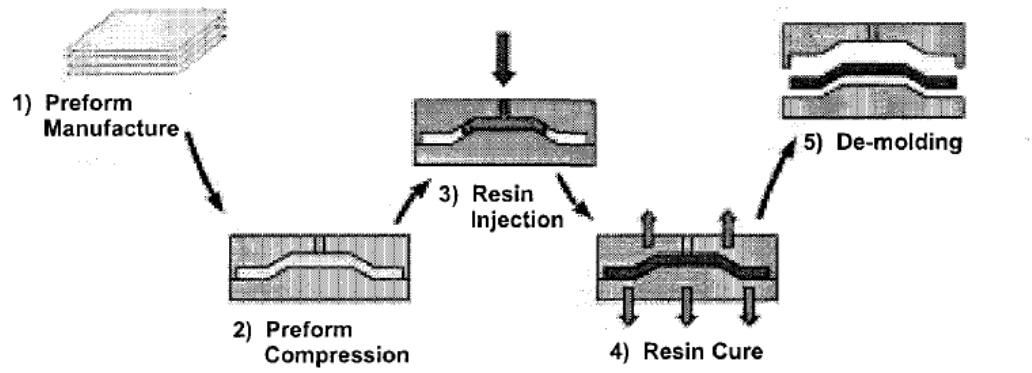

Figure 2.5 - Schematic of RTM process steps (Advani and Murat 2003)

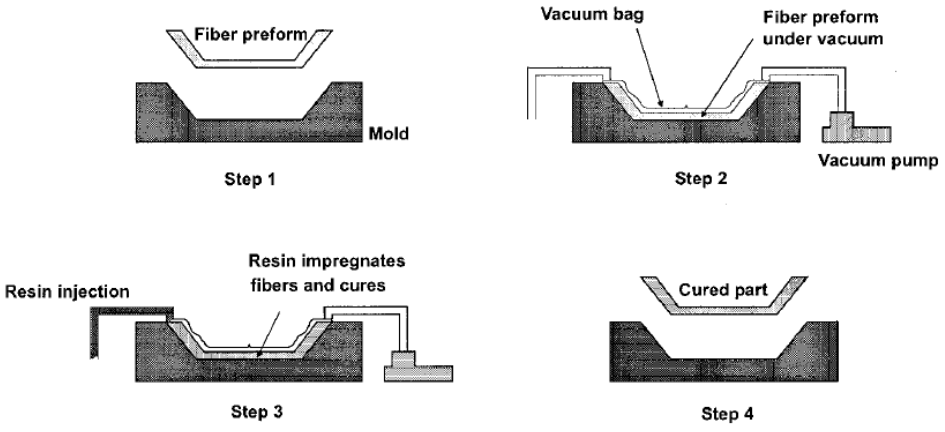

Figure 2.6 - Schematic of VI process steps (Advani and Murat 2003)

Resin Transfer Moulding has been used in the past decades for maritime, automotive and aviation purposes. The interest in this manufacturing process comes from the possibility of manufacturing complex composite structures with high consistency, tight geometrical tolerances and mechanical properties that can be compared to the ones achieved by autoclave processing. Also, Class A surface finish can be achieved on all sides of the component, which is a very important aspect for the automotive sector. However, this manufacturing presents cycle times that are not compatible to a high volume production. In fact, since cycle times in RTM can be as long as 30-120 min, depending on the resin system used. This means that the range of parts to be produced in a year corresponds to 30 000 - 50 0000 (Khoun *et al.* 2012).

In order to reduce cycle times in RTM, recently the automotive industry opted for a modification to the RTM process. By injecting resin inside the mould at pressures up to 150 bar (contrarily to the maximum 30 bar in traditional RTM), combined with faster curing resin systems, cycle times of <5-10 mins can be achieved (Khoun *et al.* 2012; Campbell 2004).

This improvement in cycle times is the flagship of this new process denominated High Pressure Resin Transfer Moulding (HP-RTM), since the advantages of conventional RTM are still maintained in HP-RTM.

2.3 Permeability

In LCM processes, as mentioned previously, after mould closure a liquid resin is injected into the mould cavity, in order to impregnate a mould preform. After the resin cures, the composite part is extracted from the mould.

In order to manufacture good quality products, the fibre preform must be completely saturated with resin. However, as part geometries get more complex, the probability of appearance of dry spots (regions not covered by resin) increases, which can lead to part rejection or repairs. To avoid these problems, a correct placement of injection inlets and air vents is paramount.

Since the beginning of LCM, this process layout optimization was conducted by trial and error, which resulted in high costs. More recently, with the development of mould filling simulation softwares, the process optimization can be done with much less costs and higher accuracy. Indeed, these softwares allow one to predict resin flow front shapes, pressure and velocity fields, as well as mould filling time (Bruschke and Advani 1990). However, a complete material properties characterization is necessary to run those simulations accurately. One of the most important properties to input in the software is permeability(Šimáček and Advani 2004).

2.3.1 Flow through porous media

The study of this kind of phenomenon was initiated by Darcy (1857) in an experiment, where a flow of water passed through sand, he then established that flow rate, pressure drop and area cross section are proportional.

$$Q = -K_h . A . \left(\frac{dP}{dx}\right) \tag{2.1}$$

It's observable that the constant K_h (hydraulic conductivity) acts as the proportionality term between all the other factors. However, hydraulic conductivity is dependent on the properties of the fluid and the porous media geometry. So, to conduct an analysis on porous media, the use of hydraulic conductivity it's not practical, therefore it's necessary to have a constant that is independent from the fluid properties.

As Scheidegger (1974) reported, hydraulic conductivity of porous media depends both on the fluid properties and the porous material properties. So, in order to have a more scientific approach, it's useful to separate both porous material and fluid properties into different variables.

That way, permeability is defined by:

$$K = K_h . \mu \tag{2.2}$$

Where:

K_h is hydraulic conductivity;
μ is the fluid viscosity.

Although Darcy's law was developed empirically, Neuman (1977) proved that it's possible to derive Darcy's law from the Navier-Stokes equation, by volume averaging theory.

He also proved theoretically that Darcy's law is only applicable where there is homogeneity in the porous medium, with respect to porosity, if the flow is done at very low Reynolds numbers (Stokes Flow) and if the fluid is incompressible.

However, these requirements can be relaxed for the case of micro-level flow, where the scale of the representative elementary volume is so small, that the variation of the fluid density or the medium porosity is not significant.

Expanding Darcy's law from 1D flow, to 3D flow, we get the following expression:

$$u = \frac{\boldsymbol{K}}{\mu} . \nabla P \tag{2.3}$$

Where:

u is the volume averaged velocity vector;
K is the permeability tensor;
μ is the fluid viscosity;
∇P is the pressure gradient.

All the complex interactions between the flow and the porous media are therefore condensed into the permeability tensor K.

2.3.2 Experimental permeability determination

As explained previously, permeability reflects the resistance a porous media offers to a fluid flow. Because in this case the resin flow is processed three dimensionally and also because permeability in fibre preforms is usually anisotropic, permeability can be written as a tensor:

$$\boldsymbol{K} = \begin{bmatrix} K_{xx} & K_{xy} & K_{xz} \\ K_{yx} & K_{yy} & K_{yz} \\ K_{zx} & K_{zy} & K_{zz} \end{bmatrix} \tag{2.4}$$

This permeability tensor is usually diagonalized, in order to obtain the three principal permeability values of the fibre reinforcement. It was defined by convention that K_1 and K_2 are part of the plane whereas K_3 is oriented through the thickness.

Because of the anisotropic properties of the reinforcement, the flowing pattern will be an ellipse oriented at an angle β, which is defined as the angle between the warp direction and the principal flow direction (Vernet *et al.* 2014).

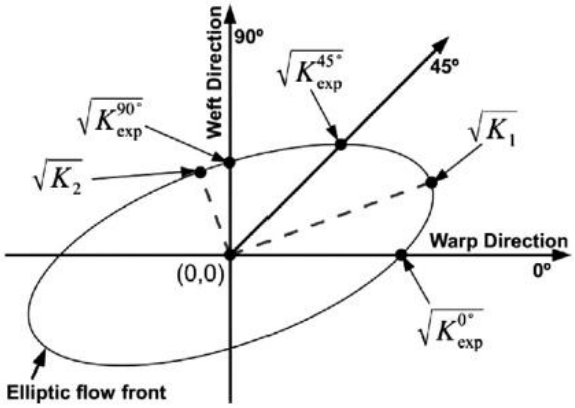

Figure 2.7 - Elliptic flowing pattern (Vernet *et al.* 2014)

Also, for the sake of simplicity, therefore reducing the amount of computational power needed, it's possible to reduce the flow model to 2D, for parts with a shell like geometry (Bruschke and Advani 1990; Šimáček and Advani 2004). However, when flow-enhancing distribution media is used, like in Seeman Composites Resin Infusion Manufacturing (SCRIMP) and similar processes, it's always necessary to analyse resin flow in 3D (Okonkwo 2010; Šimáček and Advani 2004). This is due to the speeding effect of the flow-enhancing distribution media, which allows a higher flow speed at the surface, for further impregnation through the preform thickness, thus allowing faster mould filling times.

That way, in order to have a complete and accurate characterization of the preform permeability, it's necessary to do experimental permeability measurements. These experimental measurements fall into two main distinct categories: rectilinear and radial tests (Rudd *et al.* 1997).

Rectilinear tests are made by injecting the fluid into the reinforcement, in one edge of the mould and constrain the flow in order to advance in a straight direction, towards an edge vent.

Typically, the setup for this test consists on a steel base (bottom mould), where a steel spacer and an O-ring seal are mounted. The steel spacer restrains deflections caused by reinforcement or fluid pressure. One must take special care when cutting and positioning the fibre reinforcement into the mould, because if there are some gaps between the preform and the side walls, phenomena such as by-pass flows, commonly denominated by "race-tracking", can occur. This kind of phenomena have a major influence on the values measured, therefore invalidating the possible results obtained. The setup can be seen in figure 2.8.

Next, a transparent top mould is assembled. The transparency is due to the need of tracking the flow front position and monitor whether "race-tracking" occurs, or not.

Pressure and temperature sensors are also coupled to the mould.

Prior to actual permeability testing, the test fluid should be evaluated, by studying a viscosity versus temperature correlation, over the range of temperatures that are going to be used.

Additional considerations rely on mould deflection that cannot be big enough to have significant influence on the values measured. Usually a 2% deflection limit, in relation to the nominal thickness of the mould, is established (Alms *et al.* 2010).

The fluid can be injected either in a constant pressure or constant flow regime.

The main advantage of this test is the simplicity of how one can prepare the experiment, as well as the ease of how the results are calculated.

However, due to the one dimensional nature of this test, in order to obtain the full flow ellipse, one must conduct three experiments, each one at different orientation angle of the fabric (Alms *et al.* 2010; Vernet *et al.* 2014).

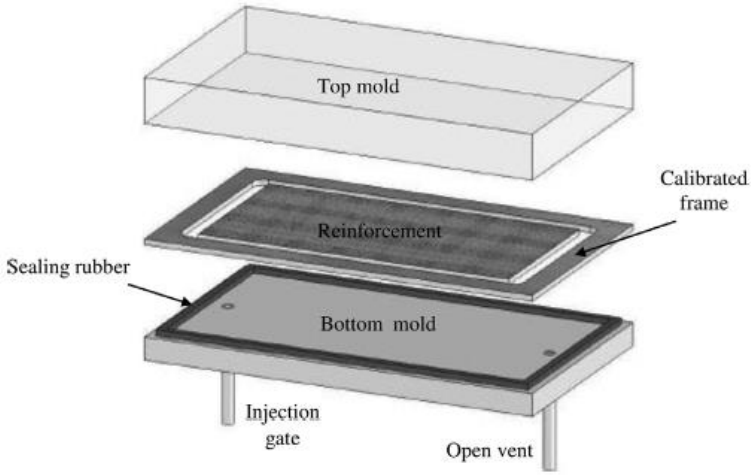

Figure 2.8 - Typical linear test mould (Vernet *et al.* 2014)

Another way to evaluate the permeability of a fibre preform, is by conducting a radial measurement. This method has some advantages over the linear testing, such as the simultaneous measurement of the two principal in-plane permeabilities and no occurrence of "race-tracking" effects.

In this setup however, the fluid is injected centrally, while inlet pressure, temperature and flow front radii are monitored. The top mould is also transparent in order to enable the flow front visualization, which can be complemented by video monitoring, in order to obtain instantaneous velocities. However, due to reinforcement compaction and fluid pressure, mould deflection containment is difficult, which usually requires secondary stiffening. This type of setup also has an added difficulty in calculating the results. These two increased difficulties have led to the abandon of this type of test, over the linear test.

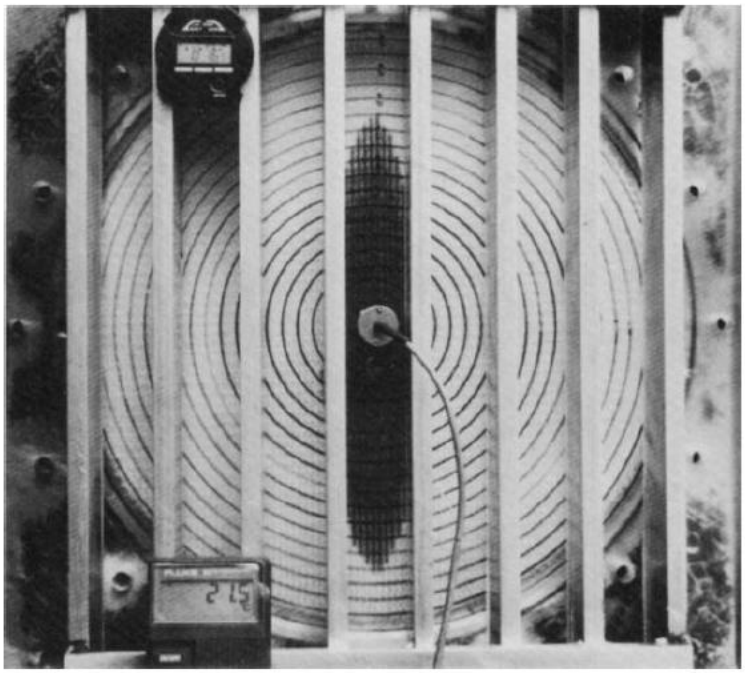

Figure 2.9 - Radial flow permeability test (Rudd *et al.* 1997)

As was mentioned previously, permeability is determined indirectly through measurements of injection pressure, flow front position and estimations of cavity thickness and fibre bed porosity. This measurements have associated uncertainties, which combined with the inherent variability in permeability, cause significant difficulties in comparing results obtained from different experimental setups, due to their high variance (Bodaghi *et al.* 2016; Arbter *et al.* 2011).

In order to solve this lack of standardization on permeability measurements, two worldwide permeability benchmarks were made. In the first one, no limitations were made on the experimental setup. This meant that 16 different experimental setups were made, using either radial injection or linear injection moulds, as well as constant flow rate or constant pressure injection. The test fluid used, was also different in many setups. The main conclusions in this study were that permeability data between participants had a scatter of more than one order of magnitude, for both reinforcements tested. This high variability in results was related to human factors, such as skilled and experienced personnel, as well as the preparation of specimens or evaluation of raw data (Arbter *et al.* 2011).

In the second permeability benchmark, several guidelines were delivered, in order to standardize the experimental procedure and therefore confirm the causes of scatter on the first benchmark. The exercise consisted in measuring in-plane unsaturated permeability of a carbon fabric, in a unidirectional setup. However, in this exercise, only three institutions weren't able to follow the recommended guidelines.

The conclusions taken were that the results had a remarkable agreement between all institutions, with the exception of the three institutions that didn't follow the guidelines. Indeed, in this benchmark, the dispersion of data between all participants is almost equivalent to the dispersion observed individually.

This meant that the human factor is not the main cause of dispersion, but in order to obtain a reproducible permeability value, it's necessary to control the test conditions, by having similar experimental setups (Vernet *et al.* 2014).

Bodaghi *et al.* (2016) also studied the most common sources of error on experimental setups and concluded that preform porosity estimation is the factor that has the biggest contribution to result uncertainty, along with pressure measurement. Since porosity estimation is dependent on many process variables, including the radius of the mould cavity, in order to reduce uncertainty even further, not only is paramount to standardize experimental setups, but also the mould design should be aim of great care.

2.3.3 Analytical permeability prediction models

Despite being paramount to process optimization, experimental permeability determination not only is costly, due to the necessity of manufacturing special moulds, but is also time consuming. For that purpose, several analytical models were developed in order to predict permeability values from the medium porosity.

These different models were created based mainly on two different approaches: lubrication theory, for low porosities and cell method for high porosities.

Lubrication theory dictates that the porous media is composed by tortuous or interconnected capillary tubes. On the other hand, cell method dictates that the fibres are spaced so far away, that in sake of practicality the media can be divided into independent cells.

One of the first models to appear, based on capillary flow through beds of spherical particles, was the Carman-Kozeny equation (Carman 1937). This equation predicts permeability values for a wide range of porosity levels, as well as different types of porous media, with reasonable accuracy.

$$K = \frac{d^2}{\psi_{CK}} . \frac{\phi^3}{(1-\phi)^2} \tag{2.5}$$

Where:

ϕ is porosity;
ψ_{CK} is the Kozeny factor;
d is the fibre or sphere diameter.

The Kozeny factor is a non-dimensional factor that for realistic porous media has to be determined experimentally. An overview of experimental and theoretical approaches in order to determine the Kozeny factor was made by Astrom *et al.* (1992). However, one of the most widely accepted methods to determine the Kozeny factor, therefore generalizing the Carman-Kozeny equation for different applications, was proposed by Carman (1937), which implements the concept of tortuosity, that is the length of the streamlines divided by the length of the sample (L_c/L).

Hence, the Kozeny factor can be written as:

$$\psi_{CK} = \phi \left(\frac{L_c}{L}\right)^2 \tag{2.6}$$

Where ϕ is the effect of particle shape, which is a fitting parameter.

Originally, in the Carman-Kozeny equation, tortuosity is assumed to be constant for the entire range of porosities and is equal to $\sqrt{2}$. The fitting parameter ϕ assumes the value of 90 in case of pipe flow or 60 in the case of slab flow.

However, this equation only applies to isotropic porous media.

According to Sadiq *et al.* (1995), the Carman-Kozeny equation has been modified to work with highly anisotropic media, like unidirectional fibre beds. Problems arise from that, because since the geometry of the flow channel was not addressed, experimental agreement has not been very consistent with the model.

Gebart (1992) also presented a model, obtained by theoretical, numerical and experimental investigation of permeability on ordered arrays of fibres. Using Navier-Stokes equation, he derived the permeability of an ordered array of parallel fibres, for both longitudinal and transverse flow directions, as a function of fibre volume fraction (V_f). It's important to notice that the solution for longitudinal flow resembles the Carman-Kozeny equation.

$$K_{transverse} = C_1 . \left(\sqrt{\frac{V_{fmax}}{Vf}} - 1 \right)^{\frac{5}{2}} . R^2 \quad (2.7)$$

$$K_{longitudinal} = \frac{8R^2}{c} \frac{(1-Vf)^3}{Vf^2} \quad (2.8)$$

Where:

R is the radius of the fibre

For square packing:

$C_1 = \frac{4}{9\pi\sqrt{2}}$;

$V_{fmax} = \frac{\pi}{4}$;

c = 57

And for hexagonal packing:

$C_1 = \frac{4}{9\pi\sqrt{6}}$;

$V_{fmax} = \frac{\pi}{2\sqrt{3}}$;

c = 53

Gebart equation parameters V_{fmax}, *C* and c have later been subject of study and modification (Endruweit *et al.* 2013), with the aim of establishing a better fit for experimental data.

Bruschke and Advani (1993) demonstrated that capillary method fails to predict permeability at porous media composed by aligned fibre arrays. They also showed that lubrication theory only gives accurate results for low porosity, as well as cell method gives accurate results for high porosity levels. So, they studied a way to create a model that could predict permeability values for all porosity levels.

For high porosity levels, they used cell method:

$$\frac{K}{R^2} = \frac{l_e}{4} \left(\ln(l_e) - \frac{3}{4} + l_e^{-2} - \frac{l_e^4}{4} \right) \quad (2.9)$$

Where:

$l_e^2 = \frac{1}{V_f}$

For low porosity levels, they used lubrication theory:

$$\frac{K}{R^2} = \frac{1}{3}\frac{\left(1-l_n^2\right)^2}{l_n^3}\left(3l_n\frac{arctan\left(\sqrt{\frac{1+l_n}{1-l_n}}\right)}{\sqrt{1-l_n^2}} + \frac{1}{2}l_n^2 + 1\right)^{-1} \quad (2.10)$$

Where :

$l_n^2 = \frac{4}{\pi}V_f$

Because this set of equations only predicts permeability for both low and high porosity extremes, Bruschke and Advani (1993) established an asymptotic model to create a closed form solution for all porosity levels:

$$M = \xi_1 M_{lubrification} + \xi_2 M_{cell\ method} \quad (2.11)$$

Where ξ_1 and ξ_2 are weighting functions responsible to create a smooth transition between $M_{lubrification}$ and $M_{cell\ method}$, in the middle range:

$$\xi_1 = 1 - e^{\tau\left(-\frac{1-\phi_{min}}{\phi-\phi_{min}}+1\right)} \quad (2.12)$$

$$\xi_2 = 1 - e^{\tau\left(-\frac{1-\phi_{min}}{1-\phi}+1\right)} \quad (2.13)$$

As one could notice, in the latter set of equations, the permeability value is normalized by the fibre radius.

2.3.3 Representative Volume Element (RVE)

Hill (1963) defined representative volume element, or RVE, as *"a sample that is structurally entirely typical of the whole mixture on average, and contains a sufficient number of inclusions for the apparent overall moduli to be effectively independent of the surface values of traction and displacement, so long as these values are 'macroscopically uniform'."*

This type of approach has been widely used in physics and mechanics of heterogeneous materials, as a way of predicting and quantifying their properties Jeulin *et al.* (2004).

When the object of study are heterogeneous materials with random dispersion of particles, a statistical analysis may be conducted in order to better understand the macro-scale final properties (Sanei and Fertig 2015; Catalanotti *et al.* 2015; Jeulin *et al.* 2004).

RVE size estimation is dependent on several factors, including the level of precision needed for the estimation of the effective property, the number of simulations one may carry out, the volume fraction of the inclusions, among others. However, if the size of the RVE is too small, the given solution may not correspond to the real properties (Kanit *et al.* 2003; Sanei and Fertig 2015).

This kind of approach can be also applied to porous media. For instance, in composite manufacturing, many studies have been conducted with the aim of predicting permeability from different porous media, resorting to the use of RVE in numerical simulations (Catalanotti, *et al.* 2015; Bird *et al.* 2014; Bergamasco *et al.* 2015; Bruschke and Advani 1993; Hwang and Advani 2010; Nabovati *et al.* 2009; K. Yazdchi 2012; K. Yazdchi *et al.* 2011).

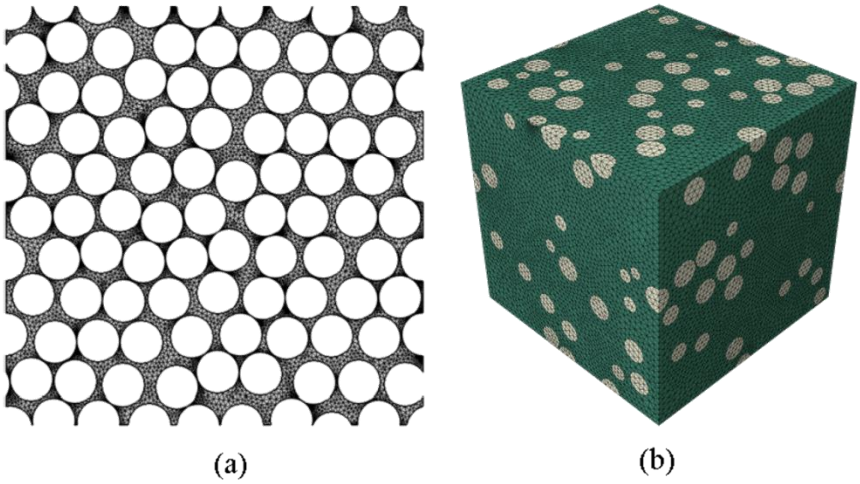

Figure 2.10 - (a) 2D RVE; (b) 3D RVE (Catalanotti 2016)

2.4 Final Considerations

From this chapter, it was possible to notice that the study of permeability has been made at two distinct scales:

Experimental permeability determination is conducted at the macro scale, where permeability is measured on the entire fibre preform, taking into account all the complex interactions between the fluid flow, the fibrous textile configuration and the component geometry. On the other hand, the analytical models target mainly the intra yarn flow, analysing the effect of the porous microstructure on permeability. They further admit that the macro-structure of the medium is a repetition of the micro-structure, so macro and micro scale permeabilities will be the same.

A third scale has also been object of study. When considering the fibre preform as a textile, one can analyse the effect that the weave pattern variation has on the fluid flow and measure permeability. The scale in which the inter-yarn permeability is measured is called the meso-scale. Endruweit *et al.* (2015) studied the effect that a non-uniform textile pattern has on permeability. To model the fibre yarns, an elliptic geometry with homogenized properties was considered. Though, the intra-yarn permeability values considered were both deterministic, for longitudinal and transverse permeability.

However, as Hoes *et al.* (2002) point out, *"The statistical distributions of the permeability and the anisotropy show that the permeability is not a material property that can be characterized by a single value".*

This means that in the case of experimental permeability determination, one needs to conduct several experiments in order to get a statistical distribution. This makes this kind of approach not only costly, but also very time consuming. Also, if one does not follow a standard procedure, result uncertainty may invalidate any application of the results.

Analytical models have the objective of aiding the task of determining permeability in a cost and time efficient way. But, although some of them provide permeability values in two directions (for anisotropic media), they fail to capture permeability variability.

A third approach is thus necessary, in order to understand how permeability is affected by the fibrous structure of the preform, with the ultimate goal of generating a capable model for process optimization, which is cost and time effective.

In order to determine intra-yarn permeability in a more realistic way, some studies perform numerical simulations in RVE with non-uniform fibre arrangements (Chen and Papathanasiou 2007; Cai and Berdichevsky 1993; Sangani and Yao 1988; Endruweit *et al.* 2013). This means that instead of the fibres being equidistant, the fibre arrangement is randomized.

The results obtained by these studies show that for longitudinal flow in random fibre arrangements, low filament density zones act as main flow channels, which increases longitudinal permeability in comparison to uniform fibre arrangements

On the other hand, for transverse flow the opposite situation can be observed. Because of the randomness in the fibre arrangement, zones with reduced filament spacing are created, which decrease the permeability of the medium (Bechtold and Ye 2003; Chen and Papathanasiou 2008; Lundstrom and Gebart 1995; Endruweit *et al.* 2013; Cai and Berdichevsky 1993).

These phenomena described above can be observed in figure 2.11.

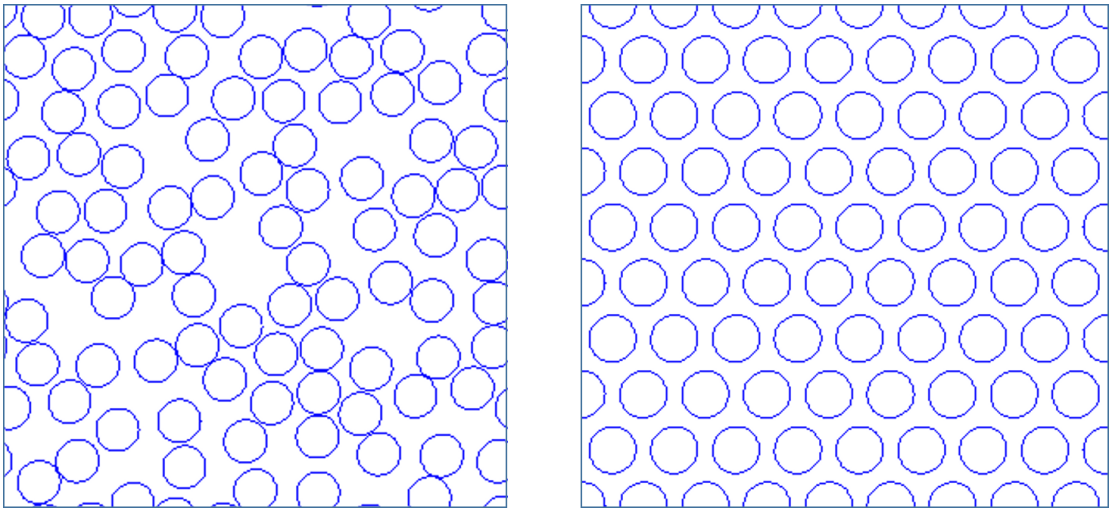

(a) (b)

Figure 2.11 - (a) RVE with random fibre distribution and (b) RVE with uniform fibre distribution (V_f=0.5)

Although these studies offer relevant conclusions, there's still a lack of a statistical characterisation of permeability, due to the small sample of results obtained. This is important, not only for the development of meso-level models with reliable intra-yarn permeability data, but firstly for development of more complex micro-level models, were local fibre clustering is considered without assuming that the fibres are uniformly distributed inside the cluster (Endruweit *et al.* 2013).

Catalanotti *et al.* (2015) studied the effect that the fibre arrangement has on transverse permeability, by conducting numerical simulations on RVEs with random fibre distribution. The conclusion reached was that the distribution of transverse permeability doesn't follow a normal distribution, by having fatter tails than the normal distribution. This implies that contrarily to common practice on experimental works, extreme permeability values cannot be ignored on the assumption of having negligible probability of occurrence.

However, it wasn't found on literature any study that analyses which stochastic model is the most appropriate to describe longitudinal permeability. Also missing from literature is a model to describe the relation between fibre volume fraction and longitudinal permeability, accounting the random fibre distribution.

The objective of this thesis is therefore to try to solve these two problems, providing a better understanding of the phenomena that govern permeability at the micro-scale.

3 Methodology

3.1 RVE Generation

3.1.1 2D RVE

Several methods for generating RVE models have been proposed. Feder (1980), Wongsto and Li (2005) and Melro *et al.* (2008) presented algorithms capable of generating RVEs with randomly distributed fibres. However they fail in achieving fibre volume fractions higher than 0.65%. Also, Wongsto and Li (2005) algorithm is not capable of creating periodic RVEs.

However, since this thesis focus on the study of intra-yarn permeability, generating periodic RVEs with fibre volume fractions higher than 0.65% is paramount.

In fact, intra-yarn fibre volume fractions have been estimated to be around 70%, but can reach higher values (Gommer *et al.* 2016; Endruweit *et al.* 2013; Cox and Flanagan 1997; Xu *et al*. 2015; Potluri *et al.* 2006). Also, with the introduction of manufacturing processes such as HP-RTM, where the textile reinforcement global fibre volume fraction tends to rise comparing to traditional RTM, the intra-yarn fibre volume fraction is also object of increase.

Catalanotti (2016) presented an algorithm that is capable of generating RVEs with randomly distributed circular particles with volume fractions up to 91%.

Varandas (2016) proposed a modification to the work of Catalanotti (2016), in which this algorithm is capable of creating RVEs with the desired width and height, having lateral geometrical boundary periodicity imposed. For 3D RVEs, an extension is also provided in order to generate RVEs with the desired ply orientation.

However, for the purpose of this thesis, a simpler algorithm was developed by Varandas (2016). This algorithm is similar to the one developed by Catalanotti (2016), were the RVE shape is quadrangular and geometrical periodicity is imposed in all edges. The size of the RVE is controlled by the number of radius of the fibres desired (N_f). This is the coefficient between the actual size of the RVE (T) and the radius of the fibre (R):

$$N_f = \frac{T}{R} \tag{3.1}$$

Another important input parameter is the fibre volume fraction.

Similarly to Catalanotti (2016), this algorithm has three different stages before the RVE is created:

- Compact RVE – All the circles are aggregated in a hexagonal packing. This is the densest form of the RVE.
- Initial RVE – The compact RVE is expanded to meet the required boundary size.
- Final RVE – The expanded RVE suffers a perturbation which displaces the fibres randomly.

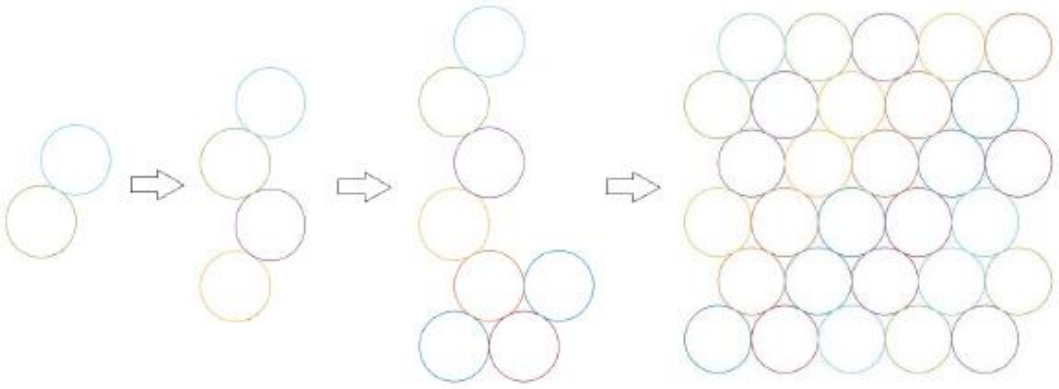

Figure 3.1 - Steps of the creation of the compact RVE (Varandas 2016)

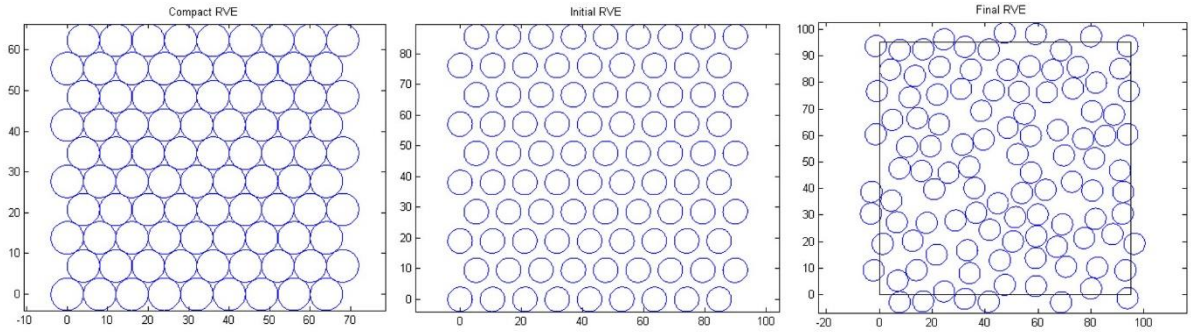

(a) (b) (c)

Figure 3.2 - Compact RVE (a); Initial RVE (b); Final RVE (c) with V_f=0.5 and N_f=24

For more detailed information about the algorithm, please consult Varandas (2016).

3.1.2 3D RVE

Since the nature of the CFD simulations to be conducted in this thesis is three-dimensional, it is necessary to convert the generated 2D RVEs to a 3D geometry. This geometry conversion operation is going to be conducted in the commercial software Abaqus®.

In order to import the RVE geometry defined in Matlab® environment to Abaqus®, a connection between these two software must be created. For that purpose, two text files (.txt) are created using Matlab® function "dlmwrite":

- new_coordinates.txt – file that contains the (x,y) coordinates of the center of the fibres;
- variables.txt – file that contains the values of the radius of the fibres, the number of fibres and the size of the RVE.

To import the variables written in the text file to Abaqus® environment and proceed with the geometry conversion operation, a python script was created (Varandas 2016).

Also, since ANSYS Fluent® is capable of reading Abaqus® input files (.inp), after the 3D RVE creation, a meshing operation is done, all coordinated by the same python script (Varandas 2016).

3.2 CFD Analysis

The CFD analysis was conducted using the software ANSYS Fluent®. For this analysis, a laminar flow regime was selected, using a pressure based solver and second order schemes, for better precision.

Since permeability, aside from fluid viscosity, is a function of fluid velocity and pressure differential, two different types of inlet/outlet boundary conditions were tested. The first is a pressure differential, where the inlet boundary condition has a higher relative pressure than the outlet. This promotes a fluid flow in the inlet-outlet direction. However, one must take care in order to input a pressure differential low enough to promote a laminar flow. This type of boundary conditions has been extensively used in permeability numerical studies.

The other option is to use a fluid velocity inlet boundary condition and at the outlet an outflow boundary condition. Outflow is a type of boundary condition where ANSYS Fluent® extrapolates the outlet pressure conditions from the specified inlet conditions, meeting conservation of mass on the continuity equation. This is a reason why this type of boundary condition can only be used in incompressible fluid flows. One must again take care, in order to input a fluid velocity at the inlet that meets a laminar regime.

After testing these two possibilities, it was possible to notice that not only the velocity inlet-outflow type of boundary conditions achieved better solution convergence, but also the computational time required was lower, for the same mesh element size. Due to these advantages, the chosen type of inlet-outlet boundary conditions for the simulations to perform, was velocity inlet-outflow.

For the other RVE surfaces, periodic boundary conditions were imposed. Also, in the surfaces representing the fibres, wall boundary conditions were imposed, with a no-slip condition.

The fluid used had constant density ρ=889 kg/m^3 and constant viscosity μ=1.06 Pa.s.

Also, the velocity chosen in order to promote a laminar flow regime was u=0.01m/s.

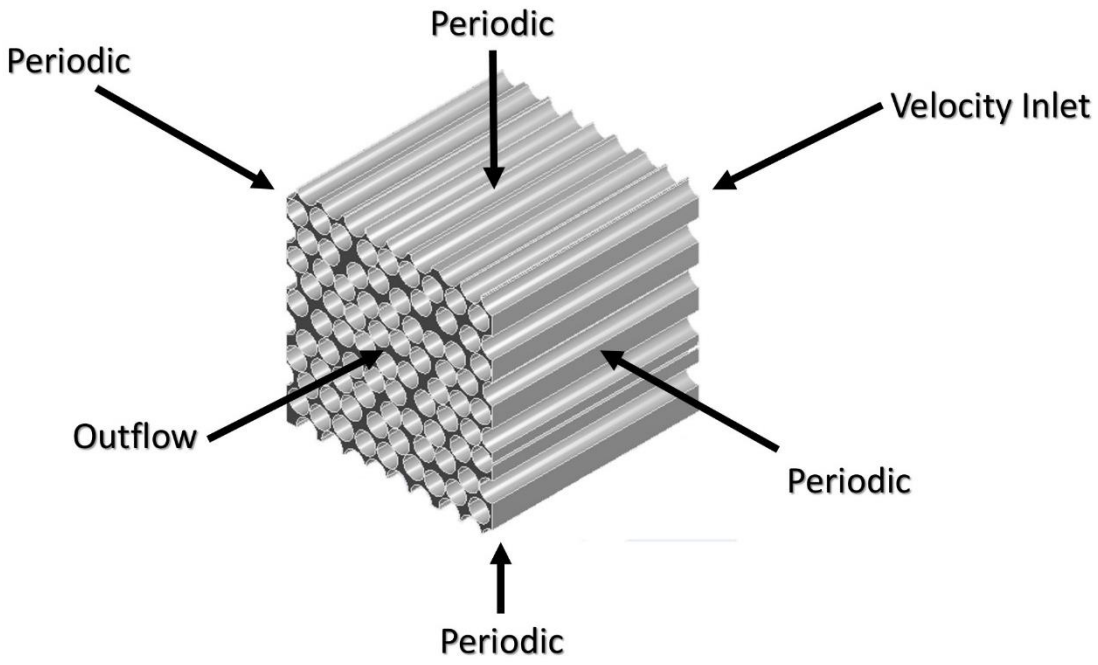

Figure 3.3 - Applied boundary conditions

The pressure results were exported as text files in ASCII format. Average velocity and mass flux values were also exported as text files (.txt).

3.3 Results Computation

Due to the need of conducting several simulations, an automation process had to be created in order to run the numerical simulations and compute results separately, since it's assumed that ANSYS Fluent® doesn't compute permeability results. For that purpose, a Matlab® script had to be created, where command line instructions were given to the analysis software, combined with the computation of the exported results.

This Matlab® routine is responsible for in each iteration loop:

- Create the 2D RVE with random fibre distribution;
- Convert the RVE 2D geometry into 3D;
- Mesh the 3D RVE;
- Generate Abaqus® Input file (.inp);
- Proceed with the CFD analysis;
- Compute permeability results;
- Export permeability results to texto file (.txt).

This means that previous works of Varandas (2016) had to be integrated in this new script, by means of a script call.

To make this algorithm do the tasks described above in each iterative loop, a while cycle was used. The use of this type of cycle presented an advantage, since some numerical simulations might present errors, but the number of computed results had to be maintained to meet the stipulated sample size.

To facilitate the scripting task, as well as give more flexibility to the automation process, the Matlab® algorithm was divided into three main modules:

- Analysis_coordinator: responsible to coordinate the automation process, by the input arguments of whether the analysis should be conducted for a given array of N_f or V_f. Also, the desired sample size should be specified in this module;
- Analysis_iterator: Called from the previous script, this module is responsible to proceed with the iteration process itself, where the interaction with Abaqus® and ANSYS Fluent® was made for the required for the number of iterations stipulated to meet the required sample size;
- Permeability_calculator: This module was responsible to compute permeability values from the exported data from the numerical simulations. The permeability results would then be stored in a text (.txt) file in a specified directory. This script would start in each iteration process in "Analysis_iterator" by a script call.

In the "Permeability_calculator" module, permeability values would be calculated by the following equation that is Darcy's law rewritten in order to permeability:

$$K = \frac{u}{\frac{dp}{dx}} \mu . \phi \tag{3.2}$$

Since in the numerical simulations the fluid velocity is controlled in the interior of the porous medium, it is necessary to account for the porous medium porosity (in Equation 3.2). This is due to the fact that in Darcy equation, the accounted fluid velocity is the one on the outside of the porous medium. By accounting the medium porosity in Equation 3.2, the fluid velocity on the outside of the porous medium is extrapolated from the velocity on the inside of the porous medium, also designated as filter velocity.

The $\frac{dp}{dx}$ factor is calculated by the differential in the average pressures on the outlet and inlet planes, divided by the RVE size:

$$\frac{dp}{dx} = \frac{\left(\left(\sum_{j=1}^{n_i} P_j\right).\frac{1}{n_i}\right) - \left(\left(\sum_{w=1}^{n_o} P_w\right).\frac{1}{n_o}\right)}{N_f.R} \tag{3.3}$$

Where:

n_i is the number of element nodes in the inlet plane;
n_o is the number of element nodes in the outlet plane;
j is the inlet node number;
w is the outlet node number;
R is the radius of the fibre.

For the simulations in question, the fibres were considered to have a radius of 4e-6 m.

As it mentioned previously, errors were detected in some simulations. When the error was due to a corrupted RVE geometry from the input file, ANSYS Fluent® was programed to close automatically and the iteration process was restarted. However smaller scale errors were also detected, which would cause major imbalances between inlet and outlet fluxes and therefore invalidate results. In order to not account those incorrect results, an "if" condition was included, which had the function of verifying if the net-flux imbalance (difference between inlet and outlet fluxes) was below 1%. If the condition was met, solution convergence was achieved and permeability results were computed and stored in a text (.txt) file.

A description of the algorithm is present in Figure 3.4.

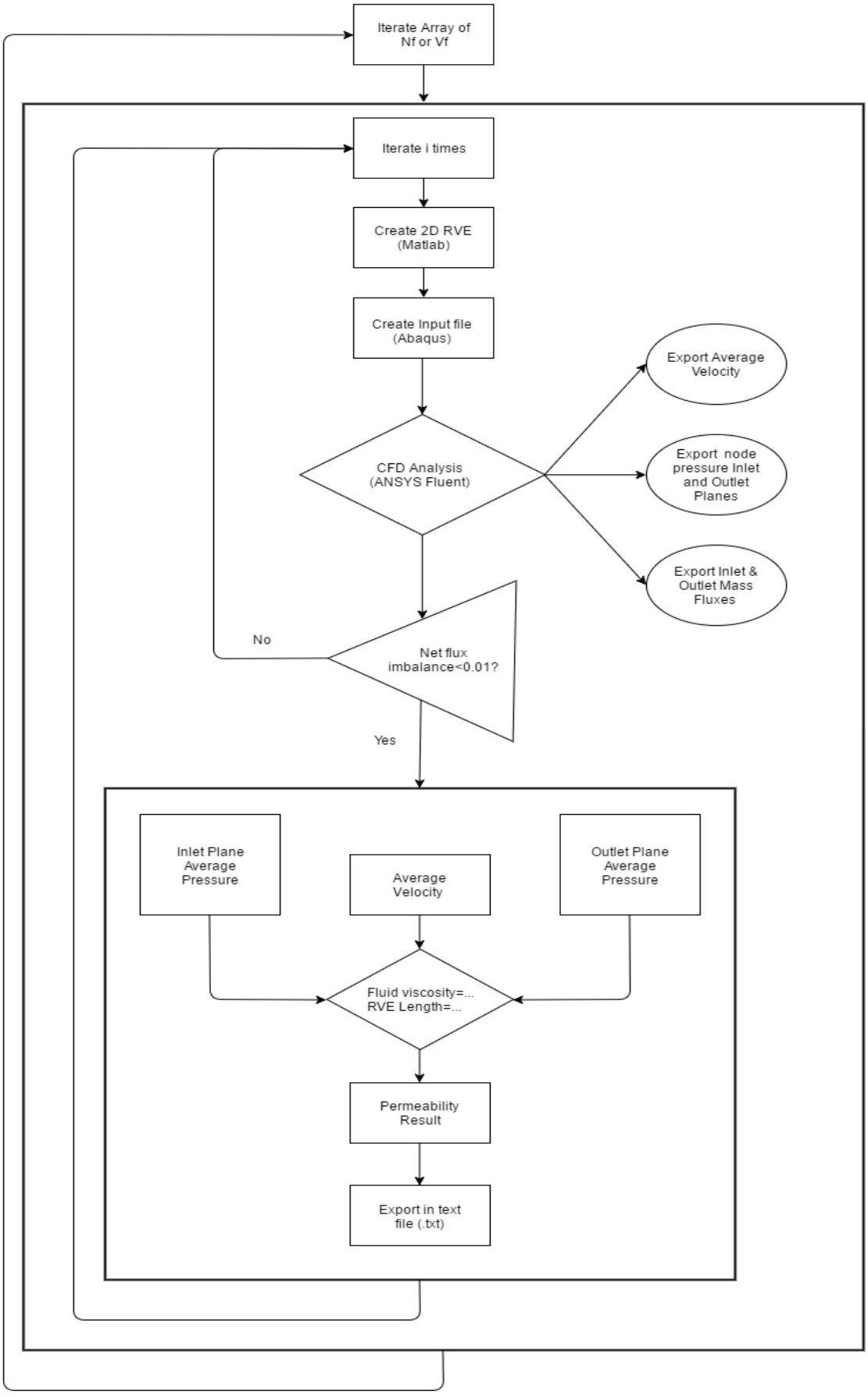

Figure 3.4 - Matlab® algorithm flowchart

In order to enable the interaction between Matlab® and the ANSYS Fluent® interface, allowing the required simulations to run in a non-graphical environment, a journal file had to be created. This journal file has the necessary commands from the Text User Interface (TUI) (ANSYS 2013) to run the simulation. Also, a command line instruction was given to ANSYS Fluent® in order to enable this program to start in a non-graphical environment.

Also, the interaction between Matlab® and Abaqus® conducted by the python script as seen previously, was initiated by a command line instruction. Similarly to ANSYS Fluent®, Abaqus® runs the required operations in a non-graphical environment (batch mode).

For a second analysis, which will be seen in the results chapter, it was necessary to modify the previous algorithm in order to compute permeability values along the RVE length. For that purpose, the ANSYS Fluent® journal file was also modified, in order to export pressure results not only in the inlet and outlet planes, but also for equally spaced interior planes along the RVE length.

Figure 3.5 illustrates how the interior planes were displaced inside the RVE.

Based on the average pressure values of each plane, the Matlab® algorithm would then sequentially compute permeability results, starting on the inlet plane, through the interior planes, and finishing on the outlet plane.

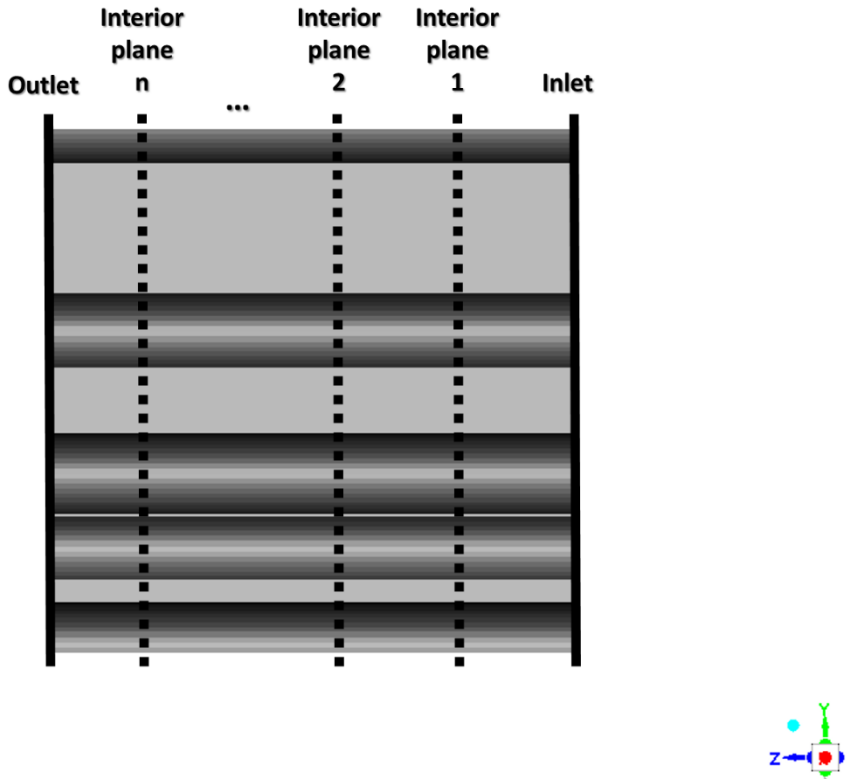

Figure 3.5 - Interior pressure planes in the RVE

3.4 Statistical Analysis

This statistical analysis is mainly intended to provide a description of permeability behaviour as a function of fibre volume fraction, quantifying its variability caused by the random fibre distribution, inside the RVE.

A necessary step in this statistical study is to verify if the experimental data follows a normal distribution model. One of the objectives of this normality test is to verify whether parametric tests can be conducted, or not. This means that if it's proven that the results sample follows a normal distribution, parametric tests can be conducted. However, if the normality condition isn't established, only non-parametric tests should be conducted (Pocinho and Figueiredo 2008; Field 2005). The advantage of using parametric tests over non-parametric is the better level of confidence that they provide.

Another reason to conduct this normality test is to have a better insight of the influence that random fibre distribution has on permeability behaviour. This influence can later be understood by analysing the statistical distribution that better represents the data generated from the numerical simulations. Though, a first step should be the acceptance, or not, of normality.

For this normality test, visual and analytical methods such as histograms, Q-Q Plots, P-P plots, Shapiro-Wilk (Shapiro and Wilk 1965) and Kolmogorov-Smirnov (Massey Jr. 1951) tests were used.

Also, for the purpose of generating a regression model, parametric and non-parametric tests were used, in order to determine which curve had a better fit to the experimental data.

This statistical analysis was made, using the commercial software IBM SPSS®.

4 Results and Discussion

4.1 CFD Simulations

It is already known that the CFD simulation in itself, doesn't give the required permeability results, since permeability is not a flow parameter in the simulation. However, a spectre of results can be obtained from the numerical simulations. From this spectre of results, for the purpose of permeability calculation, pressure and velocity contours gain a special relevance. These results can be a strong indicator if the simulation is indeed correct, or not.

Figure 4.1 and Figure 4.2 are the plots of pressure and velocity contours inside a RVE with N_f=12 and V_f=0.7.

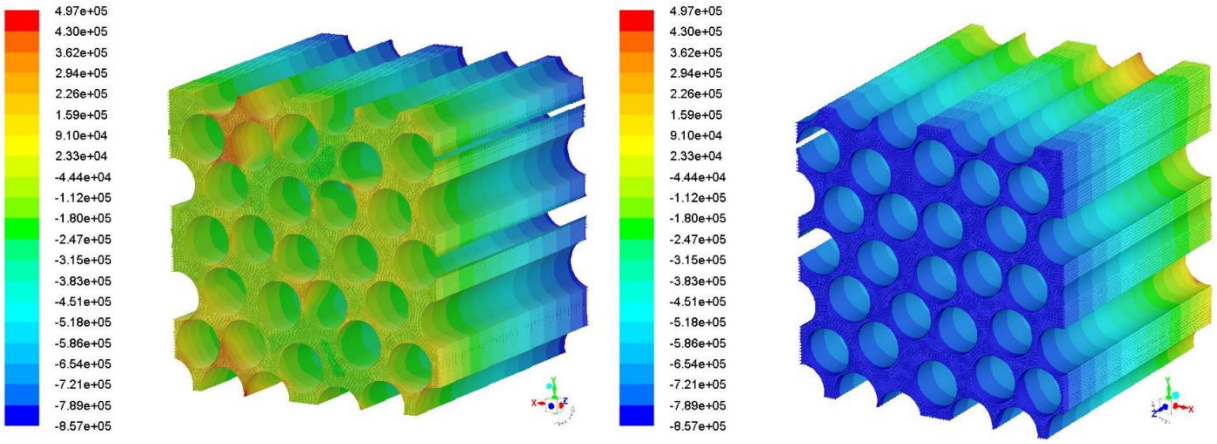

(a) (b)

Figure 4.1 - Pressure contours from Inlet plane (a) and Outlet plane (b)

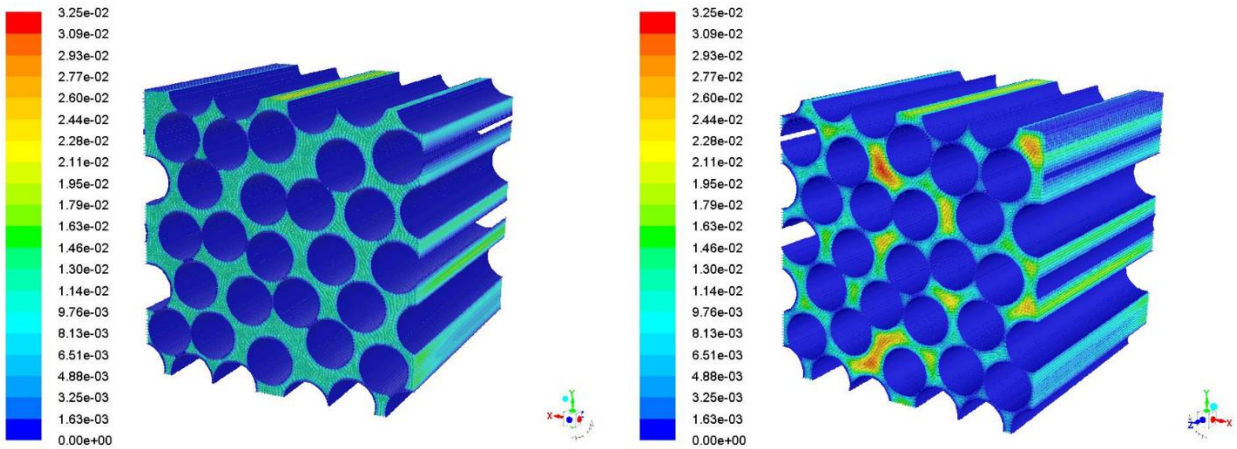

(a) (b)

Figure 4.2 - Velocity contours from Inlet plane (a) and Outlet plane (b)

On Figure 4.1 it's possible to see that a positive pressure differential is established along the RVE length (positive z axis direction). This means higher pressures at the Inlet plane and lower pressures at the Outlet plane. In this case, due to the use of the "outflow" type of boundary condition at the Outlet, it's possible to observe negative pressures in this plane. As it was referred before, this is due to the fact that the "outflow" type of boundary condition extrapolates the outlet pressure conditions from the specified inlet conditions, meeting conservation of mass on the continuity equation.

When analysing velocity contours, from Figure 4.2 it's possible to observe that at the inlet plane the fluid enters at a constant speed throughout the entire RVE section. However, along the RVE length (positive z axis direction) there's the development of a laminar flow. This can be observed with better detail in Figure 4.2 (b), where parabolic velocity profiles resembling Poiselle flow can be seen especially in areas with less fibre clustering. This is a confirmation that in RVEs with random fibre arrangements, zones with low filament density act as main flow channels (Chen and Papathanasiou 2007; Cai and Berdichevsky 1993; Sangani and Yao 1988; Endruweit *et al.* 2013).

4.2 Element Size Study

In order to ensure that the results obtained from the numerical simulations are accurate, a study of the correct element size is necessary (Cai and Berdichevsky 1993; Catalanotti *et al.* 2015). However, computational cost must be also subject of care, since the more accurate the solution is, the more costly it gets, in computational time and hardware required. So, in this study, the choice of the element size was made by a compromise between computational cost and result accuracy.

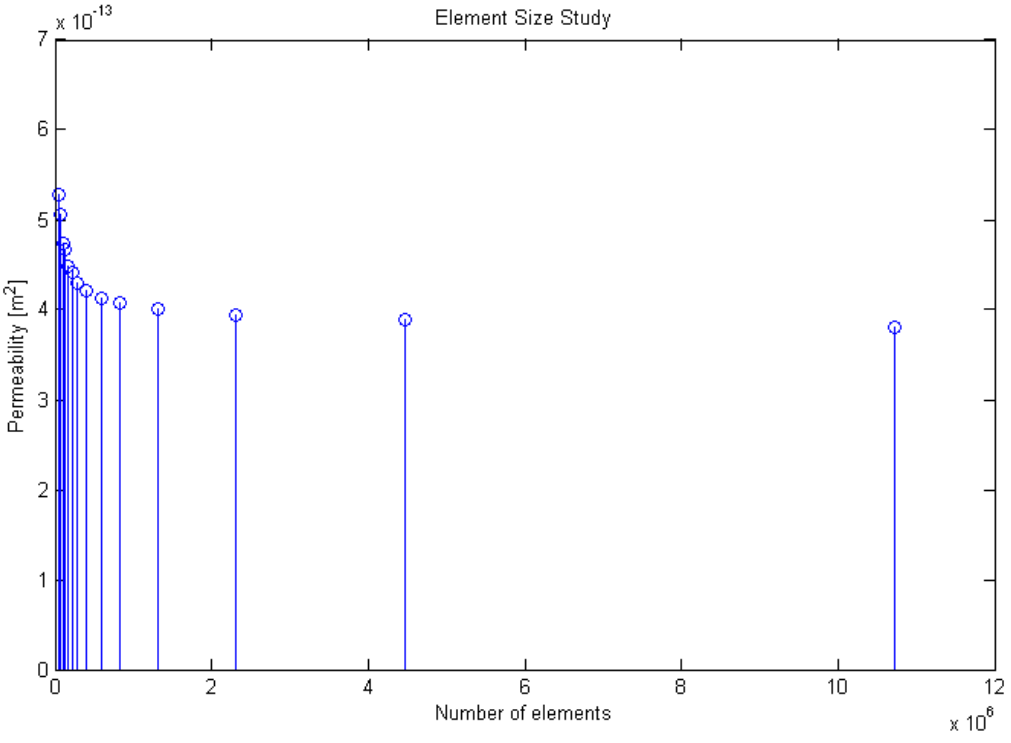

Figure 4.3 - Element Size Study for a RVE size N_f=12 and V_f=0.7

To conduct this element size study, an RVE with N_f=12 was meshed with a number of elements ranging from 55640 to 10730334. It was possible to conclude that the difference between permeability results with 220752 elements to 10730334 elements was around 13% whereas computational time was significantly lower, as well as the hardware required.

4.3 RVE Size Study

It is known that the stochastic nature of the permeability, induced by the random fibre distribution, leads to scatter in the results data.

As it has been shown by Chen and Papathanasiou (2007), Chen and Papathanasiou (2008), Catalanotti *et al.* (2015), the mean normalised permeability values $\langle K/d^2 \rangle$ and standard deviations $\sigma(K)$ obtained by the numerical simulations are not only influenced by microstructural parameters, such as porosity (ϕ), but also by the RVE size. Since the objective of this study is to measure permeability independently from the RVE size, in theory, infinitely long RVEs should be used. However, as Chen and Papathanasiou (2007), Chen and Papathanasiou (2008), Catalanotti *et al.* (2015) reported, as the size of the RVE is increased, both the expected average values and standard deviations converge.

The results presented in Figure 4.4 confirm the previous observations.

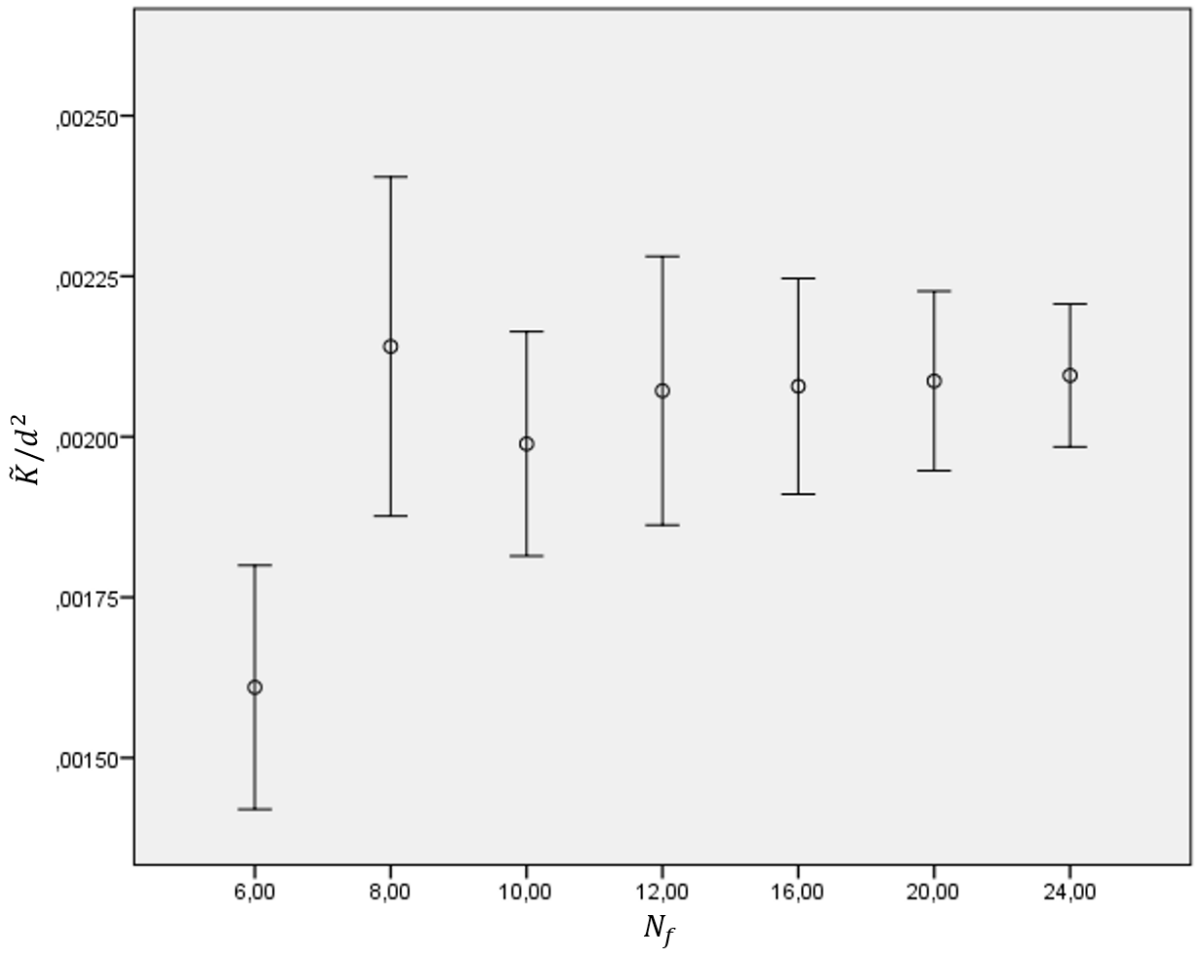

Figure 4.4 - Study of the effect of the RVE size on average permeability

For this study, 145 simulations were made for each RVE size, ranging from N_f=6 to N_f=24, with a fibre volume fraction V_f=0.7. The error bars indicate two times the standard deviations obtained. Also, in order to compare in a non-graphical way the results variability, coefficients of variation (COVs) were calculated for each RVE size.

Table 4.1 - Coefficients of Variation (COVs) for each RVE size (Nf)

N_f	Coefficient of Variation
6	5,9%
8	6,2%
10	4,4%
12	5,0%
16	4,0%
20	3,3%
24	2,7%

From Figure 4.4 and Table 4.1, it's possible to conclude that with the RVE size of N_f=24, convergence seems to be established. This is due to the small COVs presented when N_f=24 as well as the small variation of average results, in relation to a RVE size N_f=12. However, as well as in the previous element size study, a compromise between solution accuracy and computational costs had to be achieved. For that purpose, the difference of average values between RVE sizes of N_f=12 and N_f=24 was calculated. This corresponds to only 1%. However the difference of the COVs between the same RVE sizes is higher (85%).

Once again, the computational time required to perform a numerical simulation was decisive and since the time required to conduct a CFD simulation is exponentially higher in a RVE with N_f=24 than a RVE with N_f=12, the chosen RVE size for the statistical study was N_f=12.

4.4 Normality Test

To conduct the following and the subsequent statistical studies, permeability was derived from different V_f values ranging from V_f=0.5 to V_f=0.78. This range was chosen based on the works of Gommer *et al.* (2016), Endruweit *et al.* (2013), Cox and Flanagan (1997), Xu *et al.* (2015) and Potluri *et al.* (2006) which state that intra-yarn fibre volume fraction is situated around 70%.

For each V_f value, 145 numerical simulations were run, making a total of 1015 simulations.

Histograms were plotted for each V_f, with a normal probability distribution curve (in black), which can be seen in Figure 4.5.

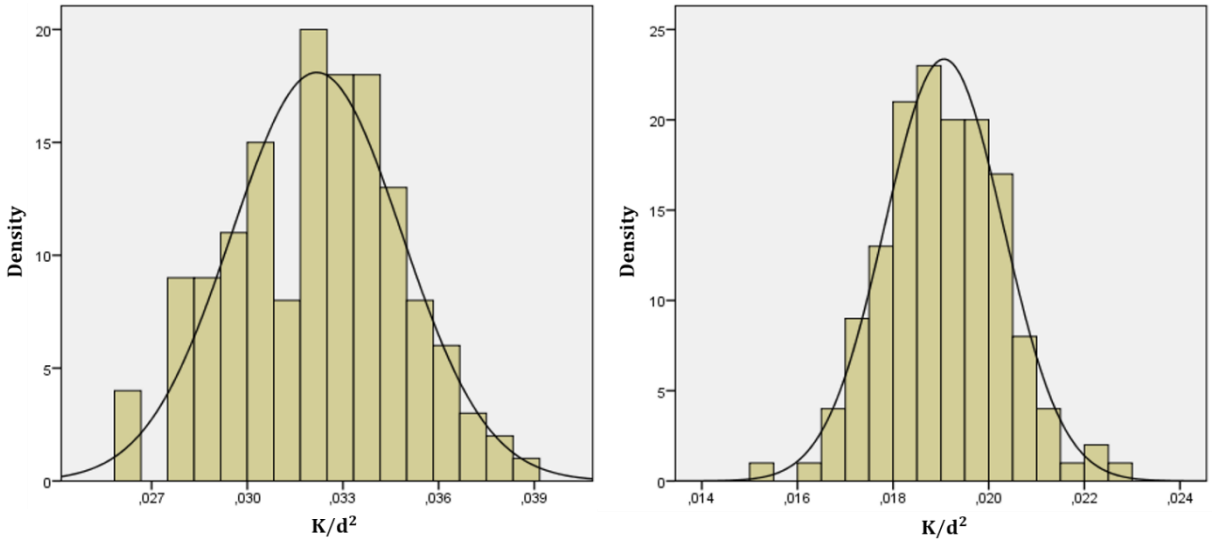

(a)

(b)

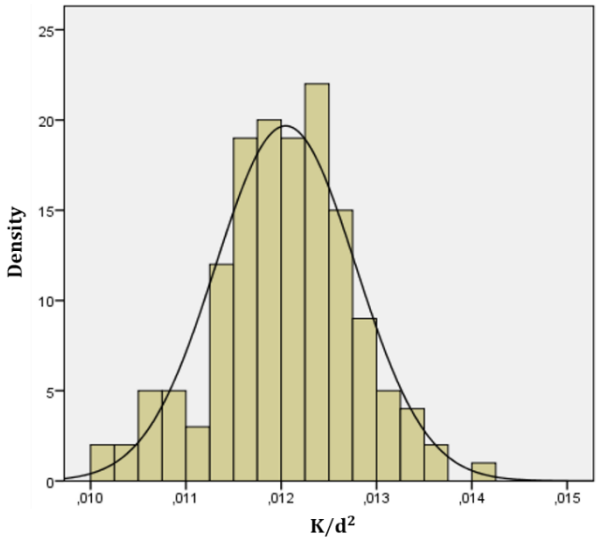

(c)

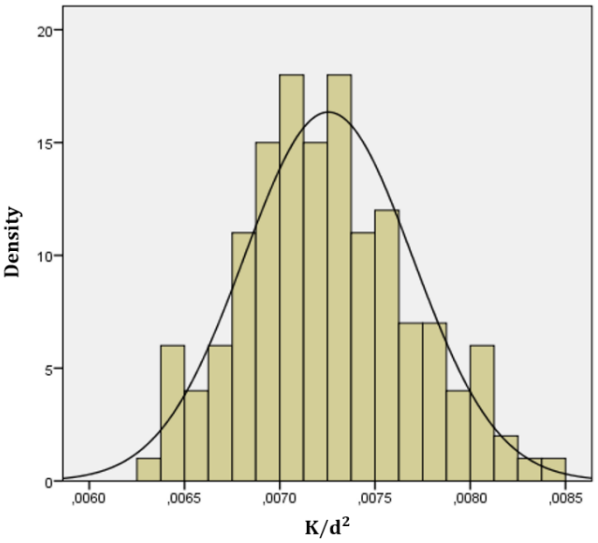

(d)

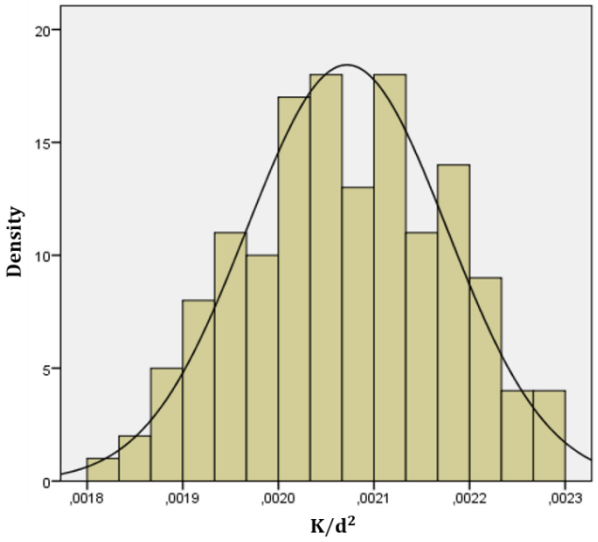

(e)

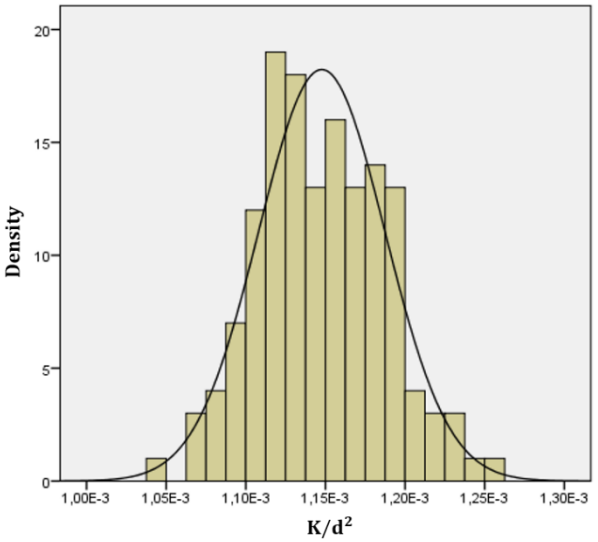

(f)

Figure 4.5 - Histograms with normal fit (in black) for V_f=0.5 (a), V_f=0.55 (b), V_f=0.6 (c), V_f=0.65 (d), V_f=0.7 (e) and V_f=0.75 (f)

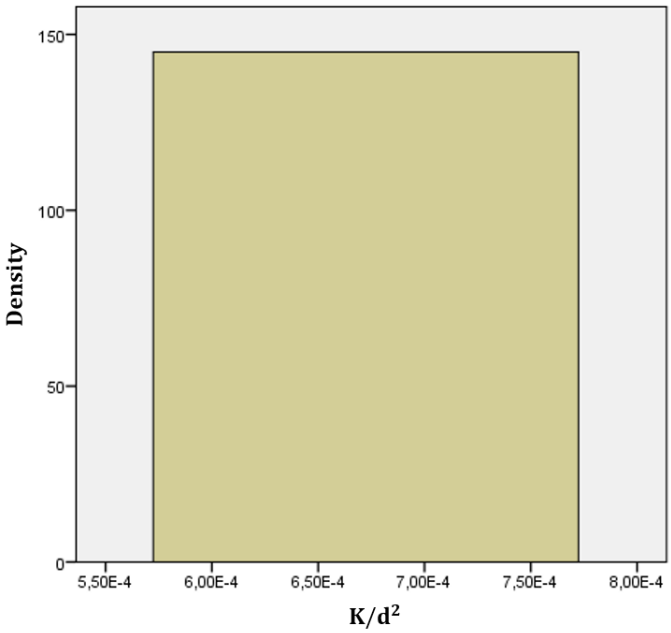

Figure 4.6 - Histogram for V_f=0.78

From Figure 4.6, it's possible to notice that the histogram for V_f=0.78 doesn't resemble the characteristic normal distribution "bell shape", contrarily to the other plotted histograms. This "bell shape" absence is due to the fact that the RVE generation algorithm has reached its limit V_f, for this RVE size (N_f=12). Though, because the RVE has reached a fibre saturation state, no random displacements are applied to the fibres. Ultimately, this means that the permeability values derived for this V_f are all equal.
As said before, for V_f ranging from 0.5 to 0.75, histograms resemble the over layered normal distribution curve (black line). However, more tests are required before assuming that the normal distribution is a correct model for longitudinal permeability.

With the purpose of verifying if the permeability data for each V_f follows a normal distribution model, firstly skewness and kurtosis were analysed.

Table 4.2 - Skewness and Kurtosis as function of V_f

V_f	Skewness	Standard Error	Kurtosis	Standard Error
0.5	-0.05	0.201	-0.402	0.400
0.55	0.116	0.201	0.302	0.400
0.6	-0.152	0.201	0.252	0.400
0.65	0.321	0.201	-0.242	0.400
0.7	-0.057	0.201	-0.639	0.400
0.75	0.179	0.201	-0.169	0.400

On Table 4.2 both skewness and kurtosis values are displayed, as well as their inherent standard error, for each V_f analysed.

On a first insight, it's possible to see that both skewness and kurtosis values are close to zero, which is the reference value for skewness and kurtosis on a normal distribution. However, for a more detailed analysis, it's necessary to convert the skewness and kurtosis values into z-scores. The process of transforming a value into a z-score can be seen in equation (4.1):

$$z = \frac{x-\mu(x)}{\sigma(x)} \tag{4.1}$$

The transformation of skewness and kurtosis values into z-scores can be done by dividing its value by its standard error (since the mean value is equal to 0):

$$z_{skewness} = \frac{S-0}{SE_{skewness}} \tag{4.2}$$

$$z_{kurtosis} = \frac{K-0}{SE_{kurtosis}} \tag{4.3}$$

By standardising these results, it's possible to compare them to already known values for the normal distribution and obtain the degree of significance. The standardised skewness and kurtosis results can be seen in Table 4.3.

Table 4.3 - Standardised values of skewness and kurtosis as function of V_f

V_f	Skewness	Kurtosis
0.5	-0.249	-1.005
0.55	0.577	0.755
0.6	-0.756	0.630
0.65	1.597	-0.605
0.7	-0.284	-1.598
0.75	0.891	-0.423

Comparing the results present in Table 4.3, to known values for the normal distribution (present in a normal distribution table), it's possible to conclude that they're all below 1.96 or -1.96, which means that there's no significant geometric deviation from the normal distribution curve ($p>0.05$) (Field 2005; Pocinho and Figueiredo 2008; Pestana and Gageiro 2014).

Since kurtosis and skewness values are in agreement to a normal distribution, to further continue this normality analysis, Q-Q plots and P-P plots were used. These plots provide a graphical way of analysing if permeability data fits a normal distribution, for each V_f, by comparing either their quantiles (Q-Q plot) or their cumulative distribution functions (CDFs).

The use of both type of plots is justified by the fact that Q-Q plots show with better detail, possible deviations from the normal distribution on the tails, whether P-P plots show with better detail, possible deviations in the middle (Wilk and Gnanadesikan 1968).

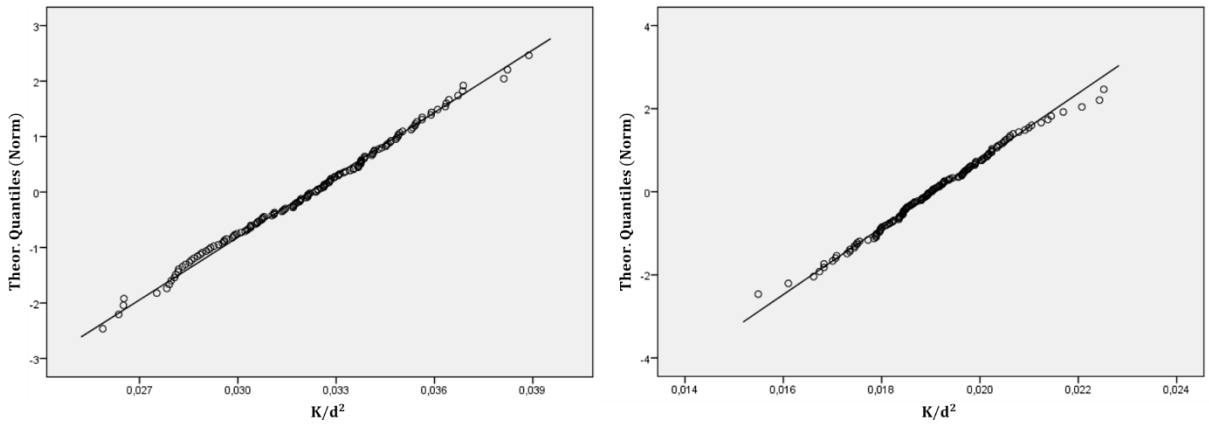

(a) (b)

Figure 4.7 - Q-Q plots for V_f=0.5 (a) and V_f=0.55 (b)

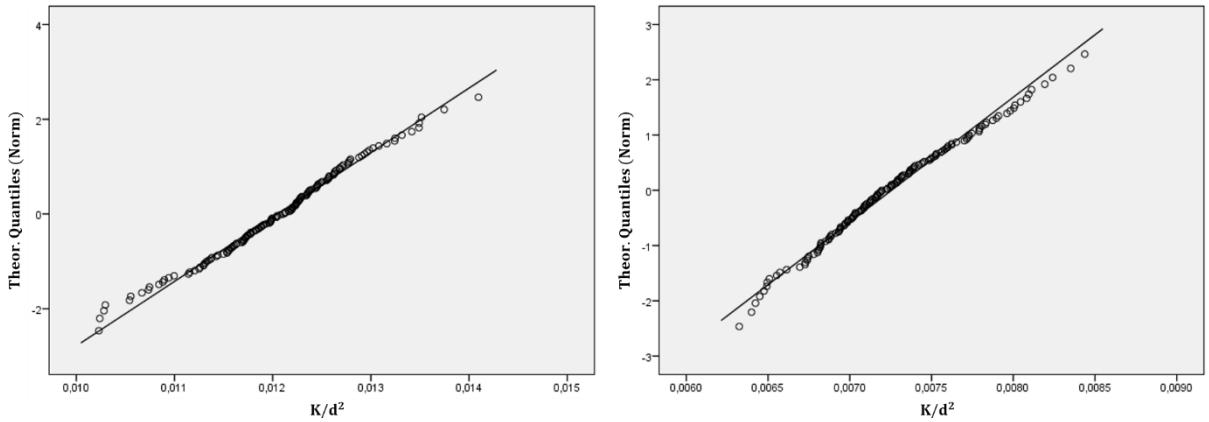

(a) (b)

Figure 4.8 - Q-Q plots for V_f=0.6 (a) and V_f=0.65 (b)

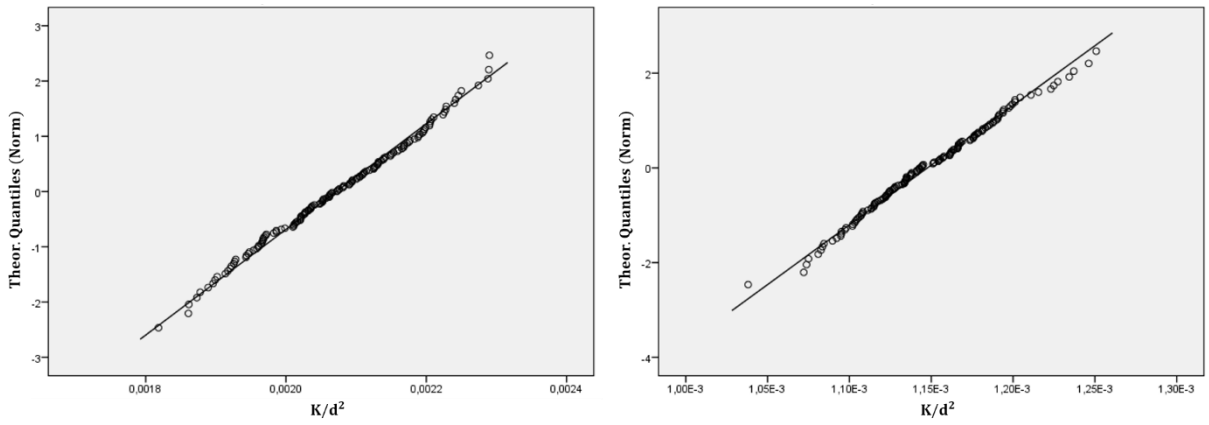

(a) (b)

Figure 4.9 - Q-Q plots for V_f=0.7 (a) and V_f=0.75 (b)

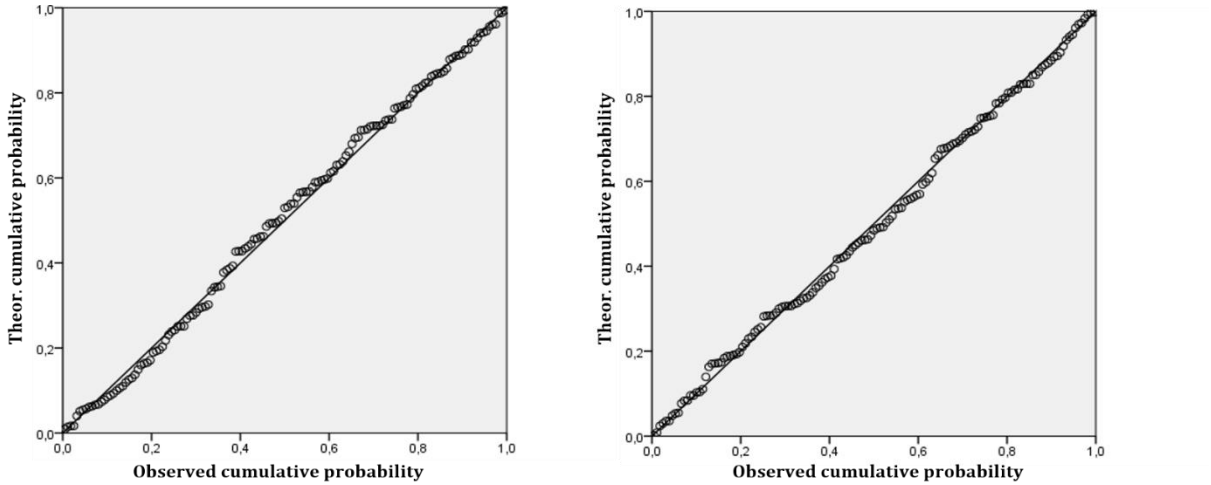

(a) (b)

Figure 4.10 - P-P plots for V_f=0.5 (a) and V_f=0.55 (b)

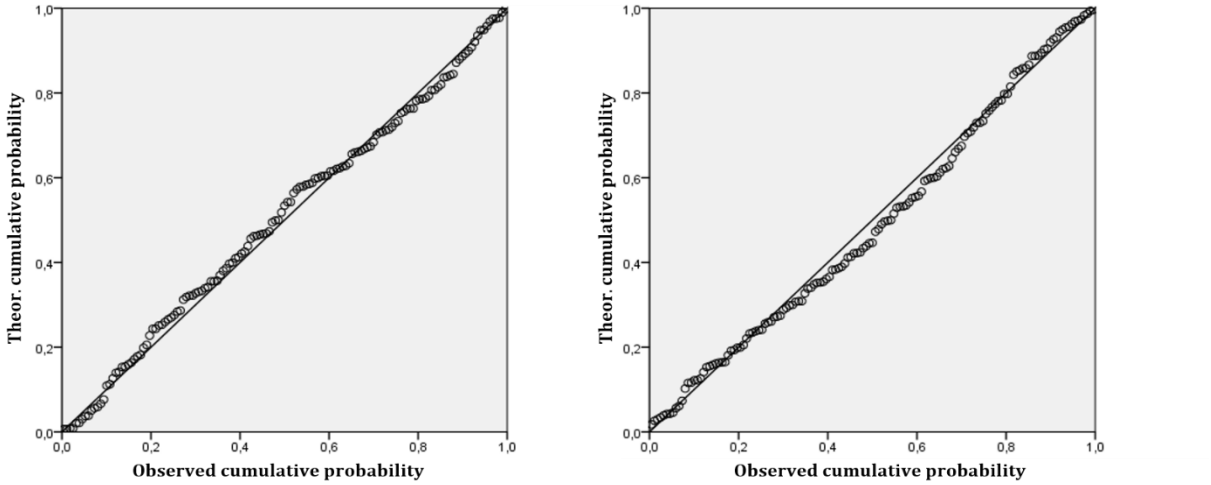

(a) (b)

Figure 4.11 - P-P plots for V_f=0.6 (a) and V_f=0.65 (b)

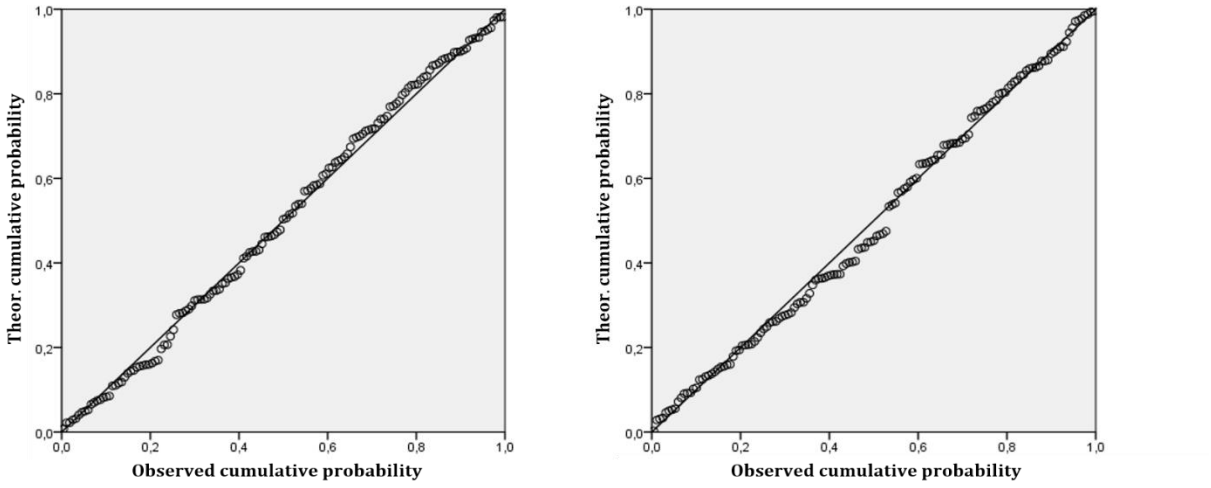

(a) (b)

Figure 4.12 - P-P plots for V_f=0.7 (a) and V_f=0.75 (b)

From Figures 4.7 to 4.12, it's possible to observe that the permeability data has no significant deviations from the normal distribution, either in the tails or in the middle. This means that the normal distribution appears to be the correct model for the permeability data.

However, in order to increase certainty that no Type I error is committed in this normality analysis, Kolmogorov-Smirnov (Massey Jr. 1951) (K-S) and Shapiro-Wilk (Shapiro and Wilk 1965) (S-W) normality tests are used.

By comparing the scores in the permeability data sample, to a normally distributed set of scores with the same mean and standard deviation, these tests tell whether the data sample distribution is normal, or not, by the significance level (p). So, for $p<0.05$, the test is considered significant which means that the distribution in question is different from a normal distribution. However, if $p>0.05$, it means that the distribution in question is not significantly different from a normal distribution (Field 2005; Pestana and Gageiro 2014).

Despite their usefulness, for samples with small size, these tests have little power to reject the normality hypothesis, which means that most often, small samples pass these tests.

However, for large sample sizes, the opposite can also be seen. In fact, when the sample size is large, these tests can give significant results, despite the deviations from normality being small.

To correct this over-sensitivity in the K-S test, IBM SPSS® uses Lilliefors correction (Lilliefors 1967), therefore rendering this test less conservative (Pestana and Gageiro 2014; Field 2005; Ghasemi and Zahediasl 2012). Table 4.4 displays the results from the normality tests.

Table 4.4 - Significance values of the Kolmogorov-Smirnov and Shapiro-Wilks tests

V_f	Kolmogorov-Smirnov (p)[a,b]	Shapiro-Wilk (p)
0.5	0.200	0.748
0.55	0.200	0.906
0.6	0.200	0.438
0.65	0.200	0.195
0.7	0.200	0.351
0.75	0.200	0.650

a. Lilliefors correction
b. This is a lower limit of the true significance

From Table 4.4, it's possible to notice that both tests reject the hypothesis that permeability data doesn't follow a normal distribution for all V_f, since all p values are above 0.05.

Since all the tests done support the hypothesis that permeability data follows a normal distribution, it's possible to conclude that the normal distribution appears to be the appropriate model to the permeability data obtained, for the V_f range in study.

Works of Hoes *et al.* (2002), Zhang *et al.* (2012), report that permeability doesn't follow a normal distribution. In order to eliminate the skewness from the distribution, a common procedure is to transform the data into a lognormal distribution, therefore getting a more symmetric distribution. However these studies were made at the macro-scale, a very important insight is given.

In fact, in this thesis, permeability is measured at an intra-yarn level, where the fibres are considered to be straight, so there's absence of any type of fibre waviness or misalignment. In these conditions, it has been established that permeability follows a normal distribution. Also, Catalanotti *et al.* (2015) report that for transverse permeability in random arrays of fibres, there's no significant skewness in the distributions.

At the meso-scale, by conducting CFD simulations on textile patterns with introduced variability, Wong and Long (2006) report that as the domain size increases, therefore approaching to the macro-scale, permeability data tends from a skewed distribution towards a normal distribution. The reason pointed out, was that with the increase of the domain size, the quantification of local inhomogeneities is lower, so the distribution gets more symmetric.

Therefore, the difference in distributions from the micro and meso-scale to the macro-scale may be explained by some phenomena that occur in experimental setups. It is known that on experimental setups factors such as porosity estimation and injection pressure control have great uncertainty associated. Also, although on a smaller scale, other factors such as fibre nesting and fluid viscosity, may contribute to the associated permeability variability (Bodaghi *et al.* 2016).

So, in order to quantify the effect that these uncertainties have on permeability, it is proposed that in future works, skewness values should be reported instead of being concealed under a lognormal transformation of the data.

Table 4.5 - Statistical characterization of permeability data, as function of V_f

V_f	K/d^2 ($\mu\pm\sigma$)	COV
0.5	0.03220±0.00266	8.3%
0.55	0.01910±0.00124	6.5%
0.6	0.01200±0.00073	6.1%
0.65	0.00730±0.00044	6.1%
0.7	0.00210±0.00010	5.0%
0.75	0.00110±0.00004	3.5%
0.78	0.00072±0.00000	0%

Table 4.5 displays the mean normalised permeability (K/d^2) values, as well as the COVs, as function of V_f. It's possible to see that permeability decreases with the increase of V_f. Also, with the increase of V_f, the COVs decrease. This can again be explained by the fact that as V_f increases, the space between fibres decreases. This means that as the available space for the fluid flow gets tighter, there's a decrease in the medium permeability. Also, this decrease in inter-fibre spacing means that the random displacements applied by the RVE generation algorithm will be shorter, therefore reducing variability in permeability, which can be observed by the decrease in COVs.

Ultimately, the limit situation of V_f=0.78 that was discussed earlier, will be reached.

By comparing the COV results with the ones obtained by Catalanotti *et al.* (2015), for transverse permeability, it is possible to understand that longitudinal permeability has less variability than transverse permeability. In fact, transverse permeability presents COV twice as big as the ones for longitudinal permeability, for the same fibre volume fraction.

The boxplot in Figure 4.13, presents in a graphical way the information discussed above.

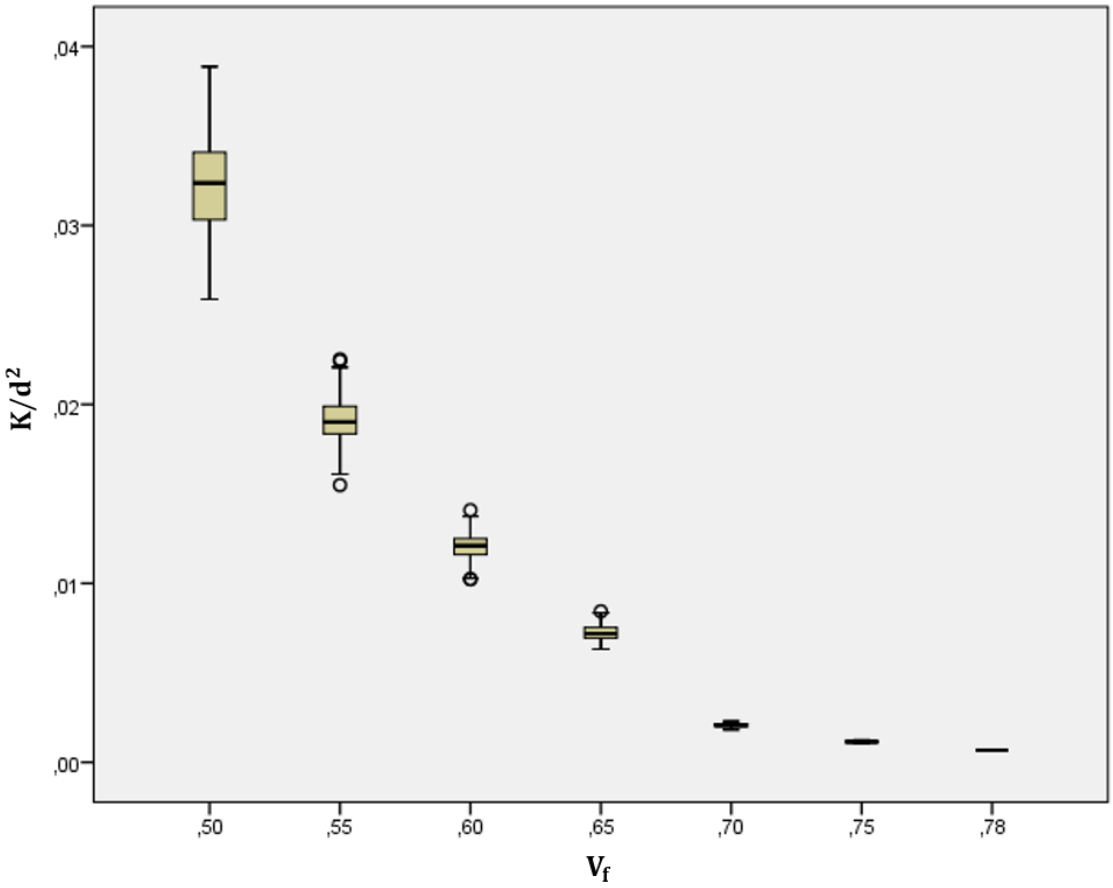

Figure 4.13 - Boxplot of permeability data

On the boxplot from Figure 4.13, the distance between the lowest horizontal line and the lowest edge of the tinted box, represents the range where the lowest 25% of the scores fall (bottom quartile). On the other hand, the distance between the top horizontal line and the top edge of the tinted box represents the range where the top 25% scores fall (top quartile). The tinted box represents the range where 50% of the scores fall (interquartile range). The thicker black line inside de box represents the value of the median. Finally, the black circles in the boxplot, represent the cases that IBM SPSS® detects as being outliers, having the normal distribution as a basis for comparison.

Permeability results obtained from the numerical simulations were compared to other numerically obtained results from previous studies of longitudinal permeability in non-uniform fibre arrays, present in the literature review (Chen and Papathanasiou 2007; Cai and Berdichevsky 1993; Sangani and Yao 1988). From Figure 4.14, it's possible to see that the deviation between the results obtained in this thesis and the results from the literature review is higher in the extreme Vf values (both for Vf=0.5 and Vf=0.75). This deviation in results may be explained by the different nature of the simulations, as well as the methods applied to create the random arrays of fibres. Indeed, the nature of the numerical simulations conducted in the previous studies is bi-dimensional. However, the numerical simulations conducted in this thesis are three-dimensional. A more detailed discussion about this topic will be done in the sub-chapter of permeability analysis along the RVE length.

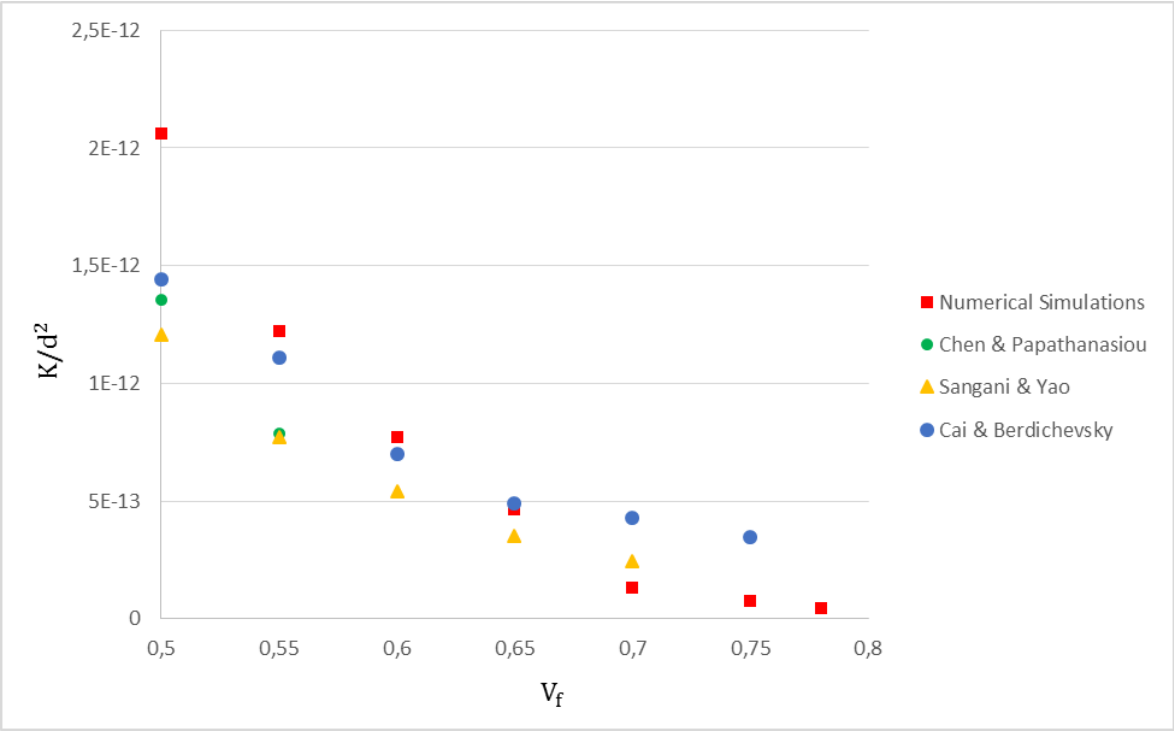

Figure 4.14 - Comparison between computed normalised permeability results and earlier computational results

4.5 Correlation between permeability and fibre volume fraction

As was referred in the state of the art chapter, there are several models that try to relate permeability, as a function of a medium porosity. Gebart and Carman-Kozeny equations get a special relevance among the other models, by being the most widely accepted ones, for the purpose in question.

However, these models suffer from a downside that is the fact that permeability was derived from a medium composed by uniformly distributed fibres, for Gebart equation, or spheres, in the case of Carman-Kozeny equation. Since previous studies (Chen and Papathanasiou 2007; Cai and Berdichevsky 1993; Sangani and Yao 1988; Endruweit *et al.* 2013; Bechtold and Ye 2003; Chen and Papathanasiou 2008; Lundstrom and Gebart 1995; Cai and Berdichevsky 1993), prove that the non-uniformity of the fibres distribution inside a RVE has a significant impact on the medium permeability, the equations in question should be aim of revision, in order to get a better adjustment to permeability derived from RVEs with a non-uniform fibre distribution.

4.5.1 Regression Analysis

In order to find the curve that better fits the numerical permeability data, a spectrum of several models was tested using IBM SPSS®. This spectrum was composed by: linear, logarithmic, inverse, quadratic, cubic, power law and exponential models.

As a way of understanding which model had the best fit to the permeability data, the R, R^2 and standard error of the estimate were calculated, for each model. It is known that R represents the correlation between the observed and predicted values of the dependent variable, in this case permeability. On the other hand the R^2, for the purpose of this study, represents the proportion of variance in permeability that can be explained by V_f. This means that the higher the R and R^2 the better is the regression model fit to permeability data. Also, lower standard errors indicate better goodness of fit.

However, it's important to remember that these indexes measure the strength of association between the regression model and permeability data, therefore not being correlation tests between permeability and V_f themselves.

Table 4.6 - Assessment of goodness of fit between each regression model and permeability data

Model	R	R^2	Std. Error of Estimate
Linear	0.938	0.880	0.004
Logarithmic	0.957	0.915	0.003
Inverse	0.971	0.944	0.003
Quadratic	0.991	0.983	0.001
Cubic	0.991	0.983	0.001
Power law	0.979	0.958	0.283
Exponential	0.988	0.976	0.214

A further graphical analysis can be done with the plot of permeability data along with the regression models. This can be seen in Figure 4.15.

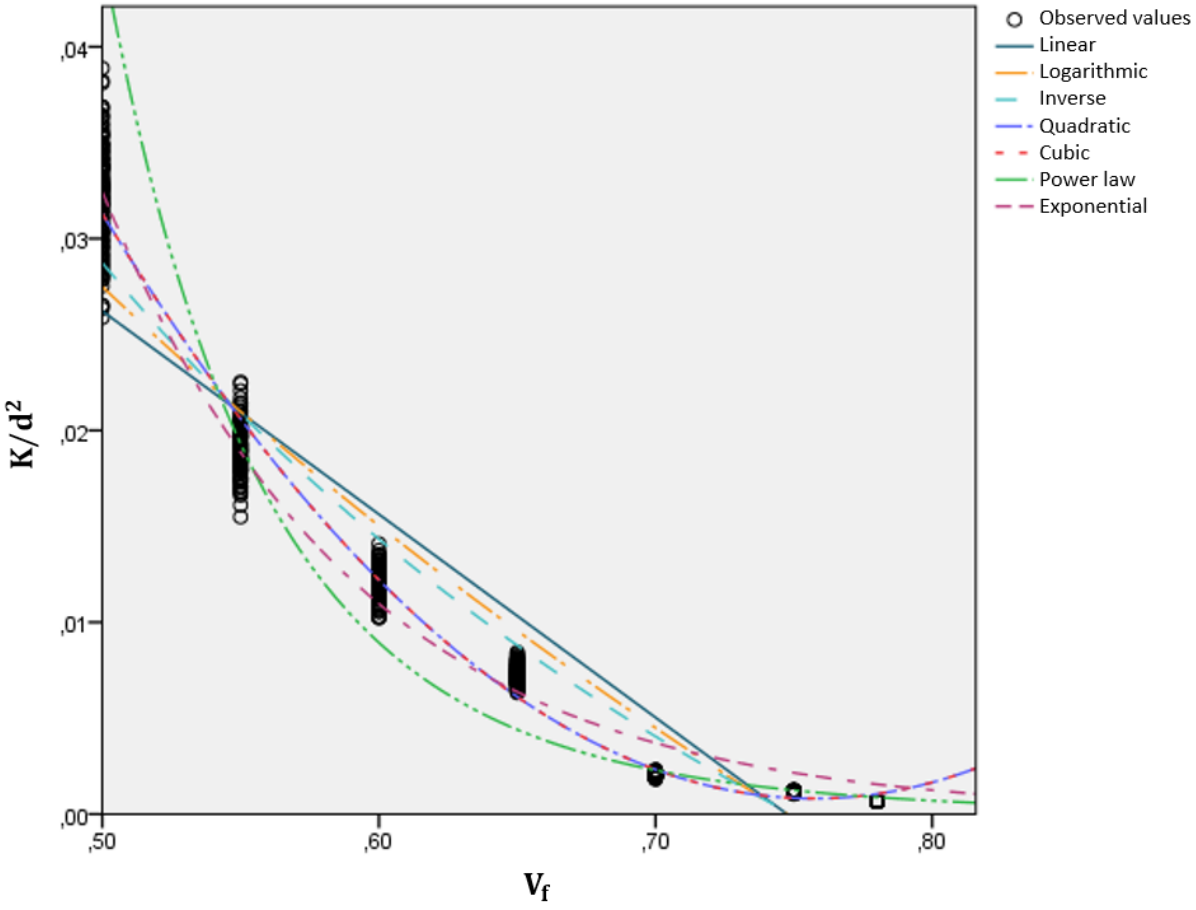

Figure 4.15 - Graphical assessment of goodness of fit between models and permeability data

From Table 4.6, it is clear that the quadratic and cubic models are the most suitable models in order to establish a relation between permeability data and V_f. However, by analysing Figure 4.15, one can observe that both quadratic and cubic models are not suitable to describe the permeability behaviour, since above V_f=0.78 permeability tends to rise. Since its known that permeability decreases continuously with the increase of V_f, both power law or exponential models should be more appropriate to establish this relation.

It is also possible to see that the quadratic and cubic regression models are not only overlapped, but their R, R^2 and standard error of estimate are equal. This is due to the fact that the equation that rules these models, for this case, is equal.

It is know that a quadratic equation has the following form:

$$y = Ax^2 + Bx + C \tag{4.4}$$

On the other hand, on a cubic equation, an x^3 factor is increased, having therefore the following form:

$$y = Dx^3 + Ex^2 + Fx + G \tag{4.5}$$

However, in this case, in order to have a better fit to permeability data, in the cubic regression model, the D factor is equalled to zero, therefore the cubic model is approached to a quadratic one.

This is the reason why both quadratic and cubic models are equal, in this study.

Since the quadratic model is therefore the one that better fits experimental data, the relation between permeability and V_f can now be written as:

$$\frac{K}{d^2} = 7{,}366 * e^{(-10{,}85 * V_f)} \tag{4.6}$$

The plot of the quadratic model with the 95% confidence interval can be seen in Figure 4.16.

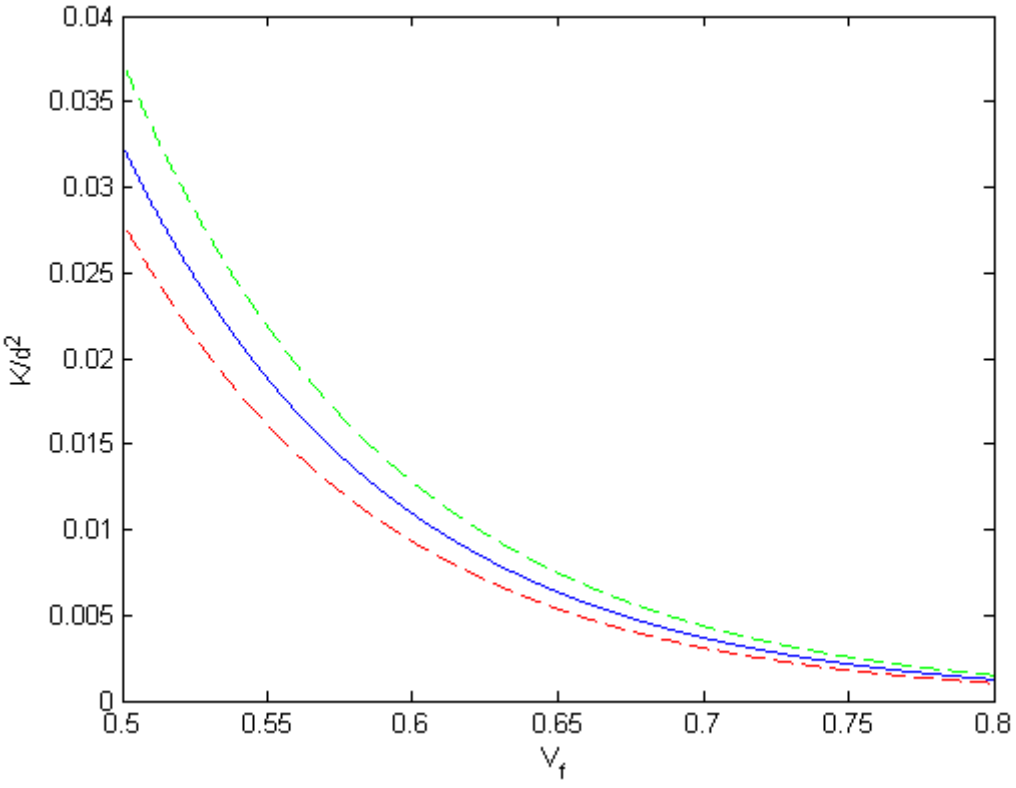

Figure 4.16 - Plot of the exponential regression model with 95% confidence upper bound (in green) and lower bound (in red)

4.5.2 Gebart and Carman-Kozeny coefficients modification for prediction of longitudinal permeability in a unidirectional fibrous medium

From the state of the art chapter, it is known that Carman-Kozeny equation can be written as:

$$\frac{K}{d^2} = \frac{1}{\psi_{CK}} \frac{\left(1-V_f\right)^3}{V_f^2} \tag{4.7}$$

Where the Kozeny factor (ψ_{CK}) is a dimensionless parameter, which is obtained empirically. By substituting equation (4.6) in equation (4.7), it is possible to determine the expression of the Kozeny factor:

$$\psi_{CK} = \frac{-0.135759.\left(V_f-1\right)^3.51534{,}2^{V_f}}{V_f^2} \tag{4.8}$$

A similar procedure can be applied to Gebart equation where before the substitution operation, it is necessary to convert Gebart equation to normalised permeability:

$$\frac{K}{d^2} = \frac{2}{c} \frac{\left(1-V_f\right)^3}{V_f^2} \tag{4.9}$$

As it is known, the c factor in Gebart equation is also a dimensionless parameter, function of the type of fibre packing.

So, proceeding with the substitution of equation (4.6) in equation (4.9), the c factor can be written as:

$$c = \frac{-0.271518.\left(V_f-1\right)^3.51534{,}2^{V_f}}{V_f^2} \tag{4.10}$$

The created analytical model was compared to the previous analytical models, proposed by Carman (1937), Gebart (1992) and Drummond and Tahir (1984). Since the last two models have specified longitudinal and transverse directions, the comparison was made between the longitudinal models.

The plotted models can be seen in Figure 4.17.

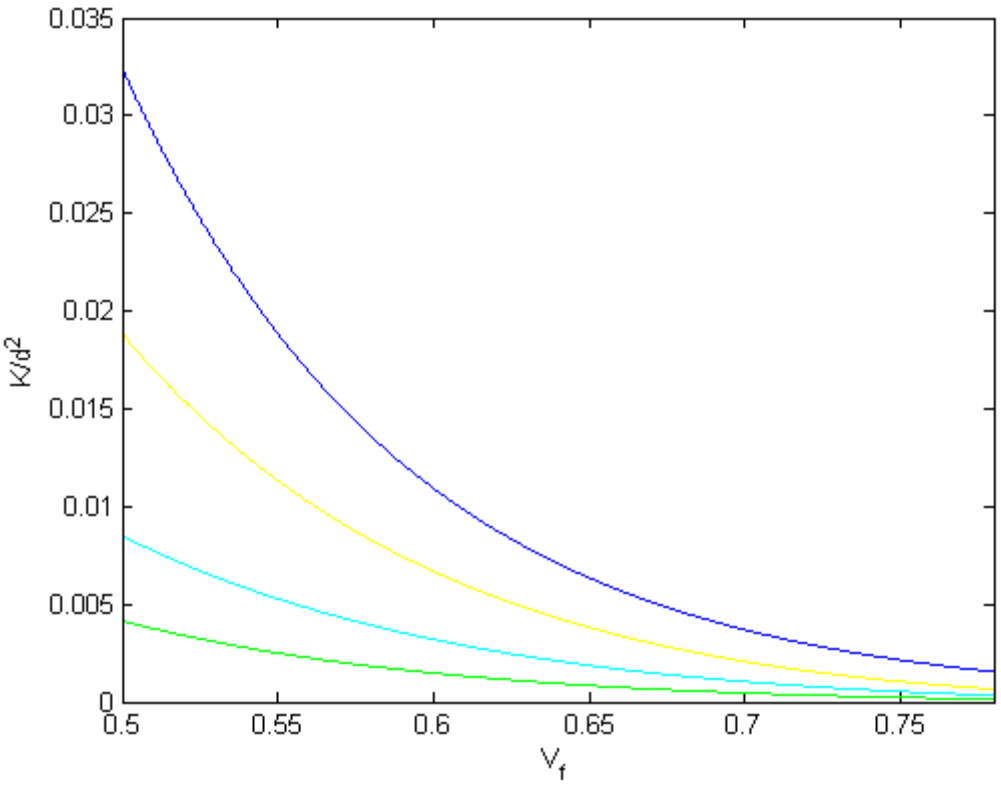

Figure 4.17 - Regression model (in blue), plotted against Gebart (1992) (in yellow), Carman (1937) (in green) and Drummond and Tahir (1984) (in cyan)

From Figure 4.17 it's possible to notice that the models converge on higher fibre volume fractions. This is due to the fact that has the fibre volume fraction increases, there's less space between fibres, therefore the random fibre arrays will be approximated to regular fibre arrangements.

The higher divergence in results for lower fibre volume fractions is in agreement with the observations made by Chen and Papathanasiou (2007), Cai and Berdichevsky (1993), Sangani and Yao (1988) and Endruweit *et al.* (2013) that state that in random fibre arrangements, low filament density zones act as main flow channels, which increase longitudinal permeability in comparison to uniform fibre arrangements.

It is important to reinforce the idea that this model is only valid for determining longitudinal permeability in unidirectional fibrous media. Also, since this model is based in the numerically obtained results, the validity of this model is constrained to the range of fibre volume fraction $0.5<V_f<0.78$. Lastly, this model only accounts for the effect of the random fibre distribution inside the fibrous medium, since there are other factors, such as the variation of the fibres diameter, which can have influence on permeability.

4.6 Pressure and Permeability Analysis along the RVE length

On the focus of this thesis, the study of permeability is done in RVEs with random fibre distribution, whose fibres are considered to be straight, therefore without any waviness or misalignments.

In order to understand the effects of fibre waviness or misalignment, permeability should be compared in a point by point basis, along the RVE length, against a model based on straight fibres. The purpose of this study is therefore establish a model for permeability along the RVE length, in the case of RVEs with straight fibres. By applying the Matlab® algorithm described in the methodology chapter, it is possible to compute average pressure values for equally spaced planes inside the RVE. The inlet and outlet planes are also included in this analysis.

In this study, 40 realizations were made for RVE lengths of N_f=6, N_f=12 and N_f=24. Also, in order to understand also the effect of fibre volume fraction, another 40 realizations were made for each V_f=0.5, V_f=0.6, V_f=0.7 and V_f=0.78.

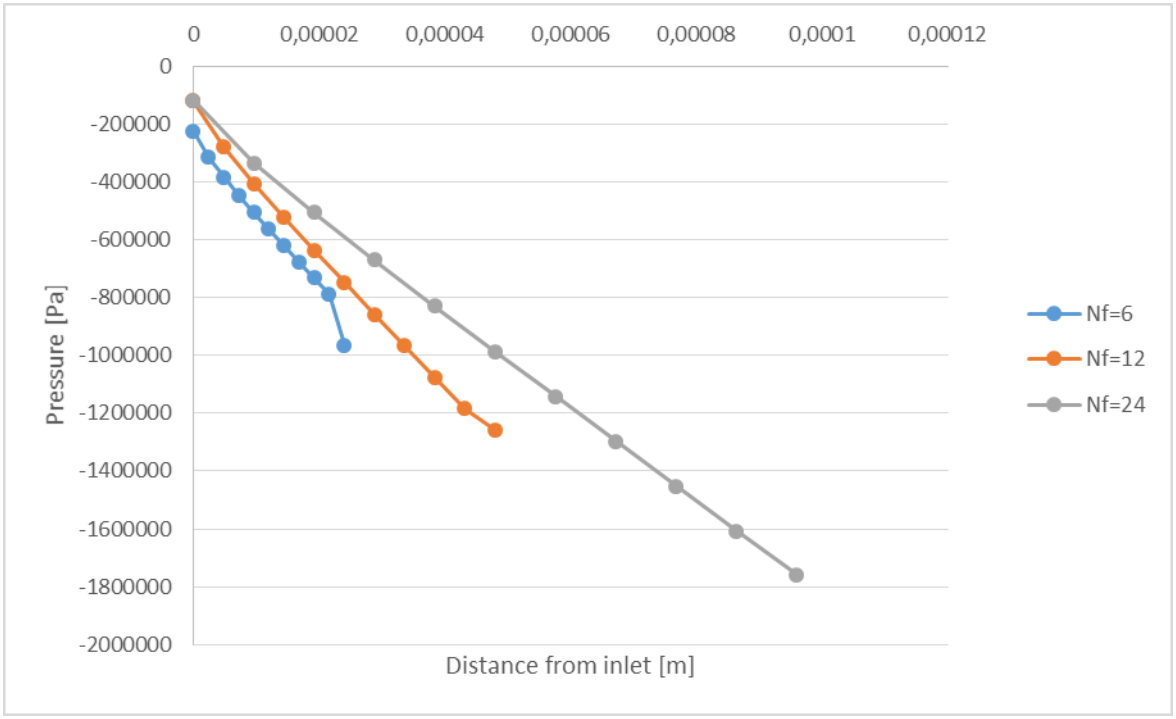

Figure 4.18 - Effect of the RVE size on pressure decay, for RVEs with N_f=6, N_f=12 and N_f=24

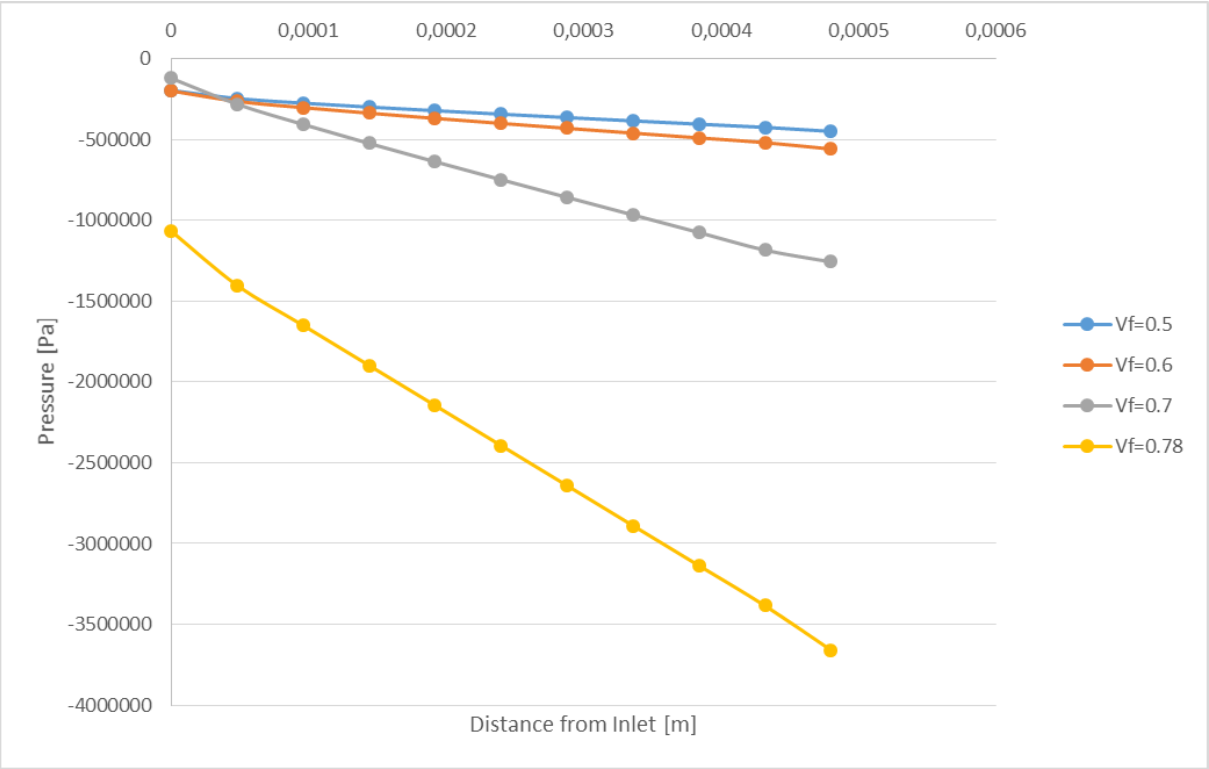

Figure 4.19 - Effect of fibre volume fraction on pressure decay, for V_f=0.5, V_f=0.6, V_f=0.7 and V_f=0.78

From Figures 4.19 and 4.20 it was possible to understand that the pressure decay along the RVE appears to be close to linear, with small fluctuations. Although the effect of the RVE size in pressure decay is not very significant, due to the small difference in the slopes of the pressure decay, it is possible to see that the effect of fibre volume fraction on pressure decay is substantial. A special attention is required to the fact that in the numerical simulations, the pressure gradient was not controlled. Therefore, only the slope of each pressure plot should be analysed.

Since ANSYS Fluent® solver controlled the pressure gradient in order to meet the required average fluid velocity inside the RVE, it is normal to obtain negative pressure values, as well as the departure from initial pressure results, in the case of V_f=0.78 (Figure 4.20). With that in mind, it's possible to conclude that with the increase of fibre volume fraction, the bigger will be the pressure decay.

Since permeability is a function of a pressure differential, between each pair of pressure planes, it's possible to compute permeability values. Therefore, permeability values were computed along the RVE length, using the average pressure values described above. Using the same 40 realizations for each RVE size and fibre volume fraction, as the ones for the pressure analysis, permeability results were computed and plotted in Figure 4.22 and Figure 4.23.

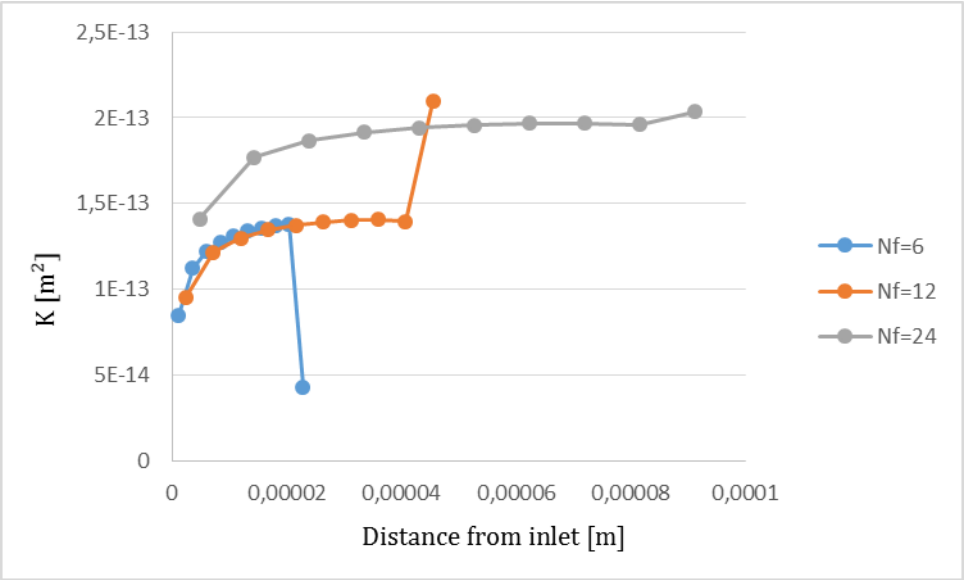

Figure 4.20 - Effect of the RVE size on permeability distribution along the RVE length

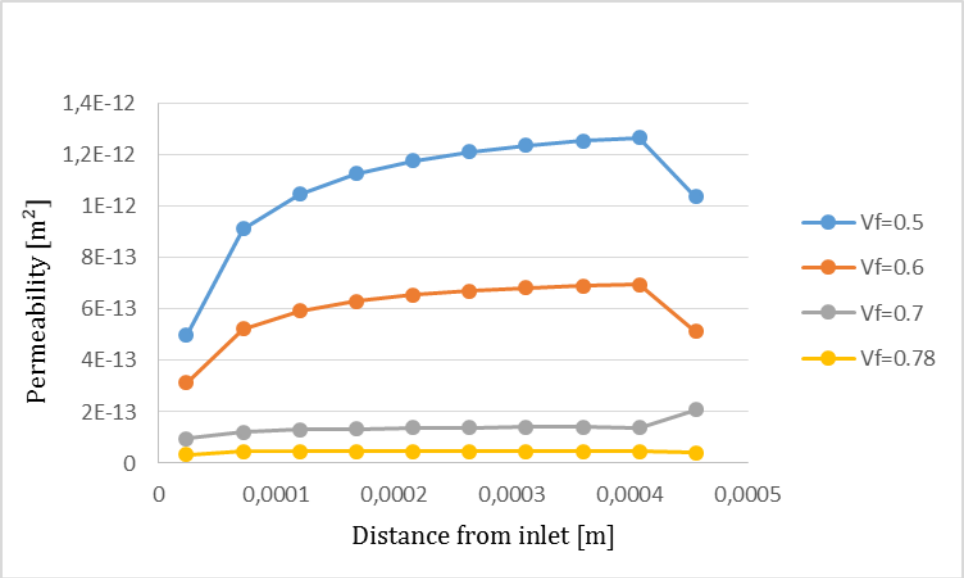

Figure 4.21 - Effect of fibre volume fraction on permeability distribution along the RVE length

From Figure 4.22 it's possible to see that permeability suffers a smoother increase with the increase of the RVE size.

Focusing on the influence of the fibre volume fraction, it's possible to see that higher V_f, cause faster permeability convergence. This may be explained by the fact that permeability is tightly linked to the development of the fluid flow, for which an analogy with the flow inside a pipe can be made. Since the length required for the development of the flow front shape, inside a pipe can be written as:

$$L_e \approx 0{,}06 R_e . d \tag{4.13}$$

Where:

L_e is distance required for the development of the flow front shape;
R_e is the Reynolds number
d is the pipe diameter

A possible conclusion is that for smaller diameters, the required distance for the development of the flow front shape is also smaller. The same happens inside the RVE, where higher fibre volume fractions cause faster permeability convergence due to the less space available for the fluid flow, therefore reaching a converged state faster. This suggests that, since in the performed numerical simulations the average fluid velocity is considered to be constant throughout the entire RVE length, inside the RVE permeability is a function of the pressure fluctuations that can be observed, which in turn these are a function of the fibre volume fraction.

In order to establish a model for the evolution of permeability inside an RVE, regression models were applied to the permeability data. By eliminating the permeability values on the extreme points of the RVE, so that the regression model doesn't account the local inhomogeneities in the flow development on the inlet and outlet, indeed it is possible to observe that permeability along the RVE length seems to follow a logarithmic function or inverse function.

Since Darcy's law, rewritten in order to permeability, takes the form of an inverse function:

$$K = \frac{u}{\frac{dp}{dx}} \mu . \phi \tag{4.11}$$

Where $u.\mu.\phi$ is a constant value, it makes sense to use a regression model, using an inverse function of the type:

$$K = A + \frac{B}{x} \tag{4.12}$$

Where:

K is permeability;
A and B are constants;
x is the distance from the inlet

Additionally, in the inverse function, when x tends to infinity, the A constant acts as the asymptote of the equation, therefore giving the converged permeability value independently from the RVE length. In the case of V_f=0.78, permeability converges almost immediately which hinders the use of a regression function. Because of this, for the sake of practicality, in the case of V_f=0.78 permeability is considered to be already converged.

So, taking Equation (4.12), in order to quantify this effect of fibre volume fraction on permeability, the A coefficients of the regression models were plotted against its correspondent V_f and a regression analysis was made in order to obtain a model for the permeability converged state.

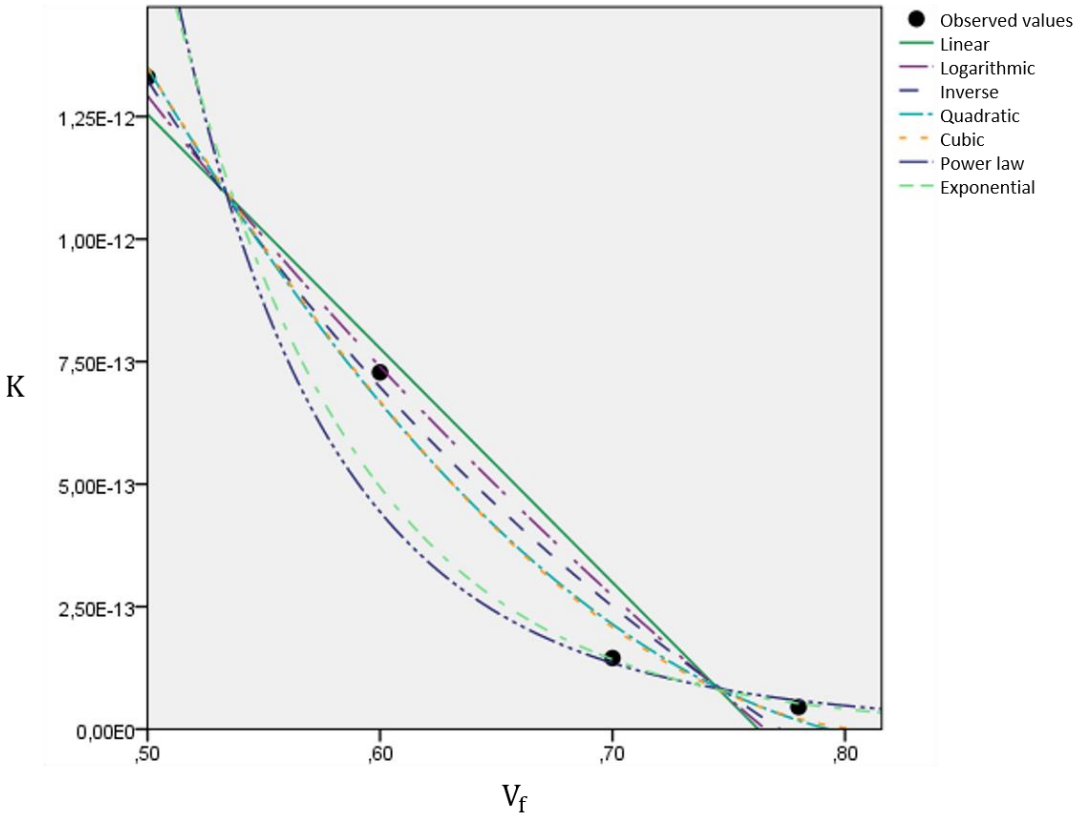

Figure 4.22 - Regression models plot for the A coefficient

Table 4.7 – R^2 factor for each regression model (coefficient A)

Model	R^2
Linear	0.954
Logarithmic	0.974
Inverse	0.984
Quadratic	0.991
Cubic	0.992
Power law	0.942
Exponential	0.966

From Figure 4.24 and Table 4.7 it's possible to conclude that both quadratic and cubic models present the best goodness of fit, for the scattered data. However, since the cubic model is the one that presents the best fit, it was the chosen model.

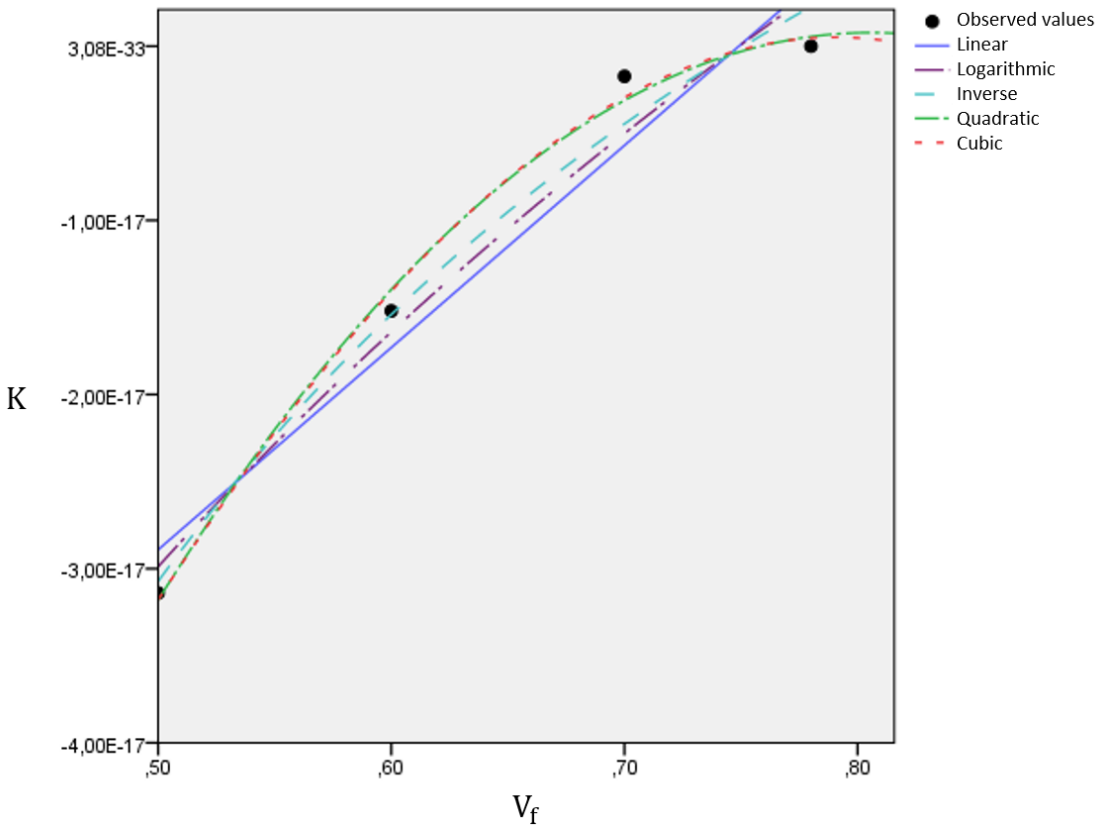

Figure 4.23 - Linear regression model plot for the B coefficient

Table 4.8 – R^2 factor for each regression model (coefficient B)

Model	R^2
Linear	0.954
Logarithmic	0.974
Inverse	0.984
Quadratic	0.991
Cubic	0.992
Power law	0.942
Exponential	0.966

From the analysis regression for the B coefficient, from the scatter plot in Figure 4.25 and Table 4.8, it's possible to see that the cubic regression model should be the best fit.

With the regression analysis done, the A and B coefficients take the following form:

$$A = 16{,}7641 * 10^{-12} - 1{,}2352 * 10^{-11} V_f + 6{,}0934 * 10^{-12} V_f^3 \quad (4.14)$$

$$B = -1{,}8088 * 10^{-16} + 3{,}4403 * 10^{-16} V_f - 1{,}833 * 10^{-16} V_f^3 \quad (4.15)$$

Since it's known that permeability as a function of distance to the inlet, takes the form of:

$$K(x) = \frac{B}{x} + A \tag{4.16}$$

Substituting the factors A and B, it's possible to get:

$$K(x, V_f) = -\frac{1{,}8088*10^{-16} - 3{,}4403*10^{-16}V_f + 1{,}833*10^{-16}V_f^3}{x} + 16{,}7641 * 10^{-12} - 1{,}2352 * 10^{-11}V_f + 6{,}0934 * 10^{-12}V_f^3 \tag{4.17}$$

When considering x to infinity, permeability will reach a converged state, whose simplified equation will be equal to the A factor:

$$K(V_f) = 16{,}7641 * 10^{-12} - 1{,}2352 * 10^{-11}V_f + 6{,}0934 * 10^{-12}V_f^3 \tag{4.18}$$

The results obtained from the permeability convergence analysis for the V_f range of $0.5<V_f<0.78$, were compared with the ones obtained in the previous section of this thesis (statistical study) and also the results obtained by Chen and Papathanasiou (2007), Cai and Berdichevsky (1993) and Sangani and Yao (1988), in Figure 4.26. Indeed one can observe that the results from the permeability convergence analysis present a much better agreement with the previous studies, for low fibre volume fractions, than the results obtained in the previous section. One reason why this may happen is due to the fact that the nature of the simulations conducted in the previous studies is bi-dimensional. Hence, this means that the length of the fibres in those simulations is considered to be infinite. In the case of the simulations conducted in this thesis, the length is finite and equal to the size of the RVE. Since for lower fibre volume fractions the convergence of permeability is slower, the length of the fibres on the RVE should play an important role in order to ensure that the fluid flow develops completely inside the RVE. With this, one could guarantee that that the computed permeability results account for a complete state of convergence.
In order to correct this over-sensitivity of the 3D simulations, it is proposed that the geometry of the RVE should be altered in future works, from a cubic shape, to a parallelepiped shape. The aspect-ratio of the parallelepiped RVE, should be a function of the fibre volume fraction since it has to take into account the length needed in order to permeability reach a converged state.

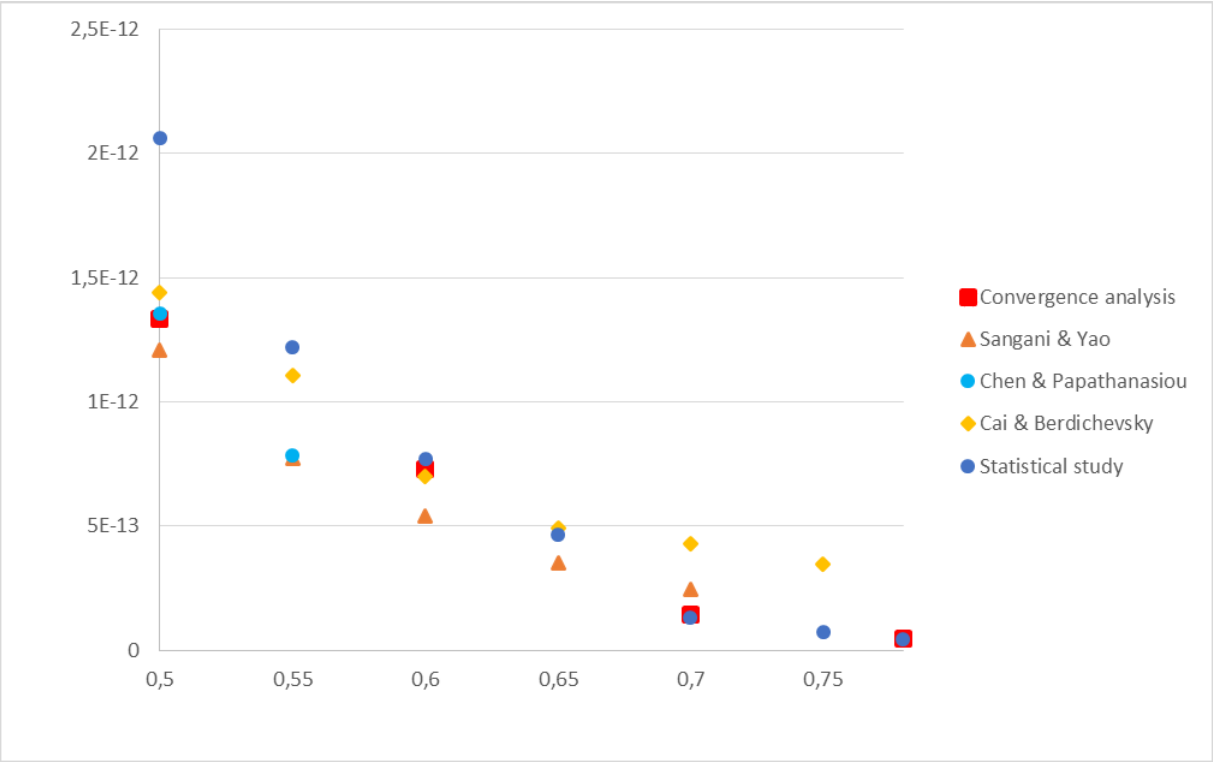

Figure 4.24 - Comparison between the results of the convergence analysis, the results from the statistical study and numerical results from Chen and Papathanasiou (2007), Cai and Berdichevsky (1993) and Sangani and Yao (1988)

5 Conclusions

Based on Darcy's law for Stokes flow through a porous medium, permeability was derived from representative volume elements composed by disordered fibre arrays. Using a Monte Carlo approach, the stochastic distribution of permeability was studied for the range of fibre volume fraction $0.5<V_f<0.78$.

The effect of the RVE size on permeability was studied. It was possible to conclude that convergence of the permeability results starts on a RVE size of $N_f=12$, where, comparing to an RVE size of $N_f=24$, the average permeability values don't suffer a significant variation. However with an RVE size of $N_f=24$, there's less result scatter, which can be observed by the coefficients of variation.

In order to understand what was the most suitable stochastic model, for the numerically obtained permeability results, a normality test was conducted. From this test it was possible to conclude that the normal distribution was indeed the best model to describe the permeability results stochastic distribution.

A regression analysis was also conducted to the permeability data, in order to revise the dimensionless parameters from Gebart and Carman-Kozeny equations.

From the point by point analysis along the RVE length, it was possible to conclude that permeability is tightly linked to the fluid flow development, reaching a steady state after a characteristic length that is a function of V_f. Also, the pressure decay was found to be approximately linear. Due to this behaviour of permeability, for the case of 3D numerical simulations, the cubic shape for the RVE may not be a suitable model, since it seems to over-predict permeability values on lower fibre volume fractions ($V_f<0.55$). Therefore, the RVE geometry should be changed to a parallelepiped shape, where the aspect ratio should be aim of study, in order to guarantee accurate results.

6 Future Works

The use of 3D numerical simulations instead of 2D sets a new objective, in order to develop more complex 3D models. Indeed, the manufacturing processes for reinforcement textiles or unidirectional plies create defects on the positioning of the fibres (waviness, crimps, deviations from the actual direction, etc.). These defects can be modelled and by deriving permeability from RVEs with these defects, their effect on permeability can be quantified.

Due to the fact that the cubic shape for the RVEs seems not to be the correct geometry for permeability analysis, the aspect ratio for a parallelepiped shape should be aim of study, in order to increase the accuracy of the results. Also, since the simulations nature is three dimensional, it's possible to retrieve information about the fluid flow in all three directions. This means that the full permeability tensor for a given RVE can be calculated in only one simulation, contrarily to what has been done. However, this process is still in a development phase, due to its increased complexity, relatively to one-directional simulations.

From the corrected Gebart and Carman-Kozeny equations coefficients, it's possible to do an upscaling operation, where meso-level models could be revisited. Since there's an analytical model relating permeability to V_f and the stochastic distribution is known to be normal, an User Defined Function (UDF) can be defined in a CDF analysis software, in order to model an averaged yarn permeability.

Finally, void formation is known to be part of LCM processing. The void formation mechanisms have already object of study at the meso-level (inter-yarn) by Matuzaki *et al.* (2015) and Park *et al.* (2011) and at a micro-level (intra-yarn) by Arcila *et al.* (2016) and Park *et al.* (2011). However, there's still room for work in order to further clarify the influence that void fraction has on permeability.

References

Advani, Suresh G., and Sozer E. Murat. 2003. *Process Modeling in Composites Manufacturing*. Marcel Dekker.

Alms, Justin B, Nuno Correia, Suresh G. Advani, and Edu Ruiz. 2010. "Experimental Procedures to Run Longitudinal Injections to Measure Unsaturated Permeability of LCM Reinforcements." *FPCM Collaborations*.

ANSYS. 2013. "ANSYS Fluent Text Command List." In , 15317:724–46. ANSYS, Inc.

Arbter, R., J. M. Beraud, C. Binetruy, L. Bizet, J. Bréard, S. Comas-Cardona, C. Demaria, et al. 2011. "Experimental Determination of the Permeability of Textiles: A Benchmark Exercise." *Composites Part A: Applied Science and Manufacturing* 42 (9): 1157–68. doi:10.1016/j.compositesa.2011.04.021.

Arcila, Ivan David, Henry Power, César Nieto Londono, and Whady Felipe Escobar. 2016. "Boundary Element Simulation of Void Formation in Fibrous Reinforcements Based on the Stokes – Darcy Formulation." *Computer Methods in Applied Mechanics & Engineering* 304: 265–93. doi:10.1016/j.cma.2016.02.010.

Astrom, B. T., R. B. Pipes, and S. G. Advani. 1992. "On Flow through Aligned Fiber Beds and Its Application to Composites Processing." *Journal of Composite Materials* 26 (9): 1351–73. doi:10.1177/002199839202600907.

Balasubramanian, M. 2014. *Composite Materials and Processing*. 1st ed. Boca Raton: CRC Press LLC.

Bechtold, Georg, and Lin Ye. 2003. "Influence of Fibre Distribution on the Transverse Flow Permeability in Fibre Bundles." *Composites Science and Technology* 63 (14): 2069–79. doi:10.1016/S0266-3538(03)00112-X.

Bergamasco, L., S. Izquierdo, I. Pagonabarraga, and N. Fueyo. 2015. "Multi-Scale Permeability of Deformable Fibrous Porous Media." *Chemical Engineering Science* 126. Elsevier: 471–82. doi:10.1016/j.ces.2014.11.065.

Bird, M. B., S. L. Butler, C. D. Hawkes, and T. Kotzer. 2014. "Numerical Modeling of Fluid and Electrical Currents through Geometries Based on Synchrotron X-Ray Tomographic Images of Reservoir Rocks Using Avizo and COMSOL." *Computers and Geosciences* 73. Elsevier: 6–16. doi:10.1016/j.cageo.2014.08.009.

Bodaghi, M., Nuno Correia, and João Machado. 2016. "Parametric Uncertainty Analysis of Permeability Data in Constant Thickness Reinforcements (RTM)." *To be published in: "Plastics, Rubber and Composites"*.

Bruschke, M. V., and S. G. Advani. 1993. "Flow of Generalized Newtonian Fluids across a Periodic Array of Cylinders." *Journal of Rheology (1978-Present)* 37 (3): 479–98. doi:10.1122/1.550455.

Bruschke, M. V., and Suresh G. Advani. 1990. "A Finite Element/control Volume Approach to Mold Filling in Anisotropic Porous Media." *Polymer Composites* 11 (6): 398–405. doi:10.1002/pc.750110613.

Cai, Zhong, and Alexander L. Berdichevsky. 1993. "Numerical Simulation on the Permeability Variations of a Fiber Assembly." *Polymer Composites* 14 (6): 529–39. doi:10.1002/pc.750140611.

Campbell, F. C. 2004. *Manufacturing Processes for Advanced Composites*. 1st ed. Elsevier Ltd. doi:10.1017/CBO9781107415324.004.

Carman, P C. 1937. "Fluid Flow Through Granular Beds." *Chemical Engineering Research*

and Design 15. Institution of Chemical Engineers: 32–48. doi:10.1016/S0263-8762(97)80003-2.

Catalanotti, G. 2016. “On the Generation of RVE-Based Models of Composites Reinforced with Long Fibres or Spherical Particles.” *Composite Structures* 138. Elsevier Ltd: 84–95. doi:10.1016/j.compstruct.2015.11.039.

Catalanotti, G., M. Bodaghi, and Nuno Correia. 2015. “On the Statistics of Transverse Permeability of Randomly Distributed Fibres.” *To be published in: "Plastics, Rubber and Composites"*.

Chen, Xiaoming, and T. D. Papathanasiou. 2007. “Micro-Scale Modeling of Axial Flow through Unidirectional Disordered Fiber Arrays.” *Composites Science and Technology* 67 (7–8): 1286–93. doi:10.1016/j.compscitech.2006.10.011.

Chen, Xiaoming, and T. D. Papathanasiou. 2008. “The Transverse Permeability of Disordered Fiber Arrays: A Statistical Correlation in Terms of the Mean Nearest Interfiber Spacing.” *Transport in Porous Media* 71 (2): 233–51. doi:10.1007/s11242-007-9123-6.

Cox, Brian N., and Gerry Flanagan. 1997. “Handbook Composites of Analytical Methods for Textile.” *NASA Contractor Report*, no. March 1997: 176.

Drummond, J. E., and M. I. Tahir. 1984. “Laminar Viscous Flow Through Regular Arrays of Parallel Solid Cylinders.” *International Journal of Multiphase Flow*, 515–40.

Endruweit, A., F. Gommer, and A. C. Long. 2013. “Stochastic Analysis of Fibre Volume Fraction and Permeability in Fibre Bundles with Random Filament Arrangement.” *Composites Part A: Applied Science and Manufacturing* 49. Elsevier Ltd: 109–18. doi:10.1016/j.compositesa.2013.02.012.

Endruweit, A., X. Zeng, and A. C. Long. 2015. “Multiscale Modeling of Combined Deterministic and Stochastic Fabric Non-Uniformity for Realistic Resin Injection Simulation.” *Advanced Manufacturing: Polymer & Composites Science* 1 (1): 3–15. doi:10.1179/2055035914Y.0000000002.

Feder, Jens. 1980. “Random Sequential Adsorption.” *Journal of Theoretical Biology* 87 (2): 237–54. doi:10.1016/0022-5193(80)90358-6.

Field, Andy. 2005. *Discovering Statistics Using SPSS*. 2nd ed. SAGE.

Gebart, B.R. 1992. “Permeability of Unidirectional Reinforcements for RTM.” *Journal of Composite Materials* 26 (8): 1100–1133. doi:10.1177/002199839202600802.

Ghasemi, Asghar, and Saleh Zahediasl. 2012. “Normality Tests for Statistical Analysis: A Guide for Non-Statisticians.” *International Journal of Endocrinology & Metabolism* 10 (2): 486–89. doi:10.5812/ijem.3505.

Gommer, F., A. Endruweit, and A.C. Long. 2016. “Quantification of Micro-Scale Variability in Fibre Bundles.” *Composites Part A: Applied Science and Manufacturing* 87. Elsevier Ltd: 131–37. doi:10.1016/j.compositesa.2016.04.019.

Hill, R. 1963. “Elastic Properties of Reinforced Solids: Some Theoretical Principles.” *Journal of the Mechanics and Physics of Solids* 11 (5): 357–72. doi:10.1016/0022-5096(63)90036-X.

Hinrichsen, Jens, and Cesar Bautista. 2001. “The Challenge of Reducing Both Airframe Weight and Manufacturing Cost.” *Air & Space Europe* 3 (3–4): 119–21. doi:10.1016/S1290-0958(01)90072-3.

Hoes, Kris, Daniela Dinescu, Hugo Sol, Marleen Vanheule, Richard S. Parnas, Yiwen Luo, and Ignaas Verpoest. 2002. “New Set-up for Measurement of Permeability Properties of

Fibrous Reinforcements for RTM." *Composites - Part A: Applied Science and Manufacturing* 33 (7): 959–69. doi:10.1016/S1359-835X(02)00035-0.

Hollaway, Leonard. 1994. *Handbook of Polymer Composites for Engineers*. Vol. 5. Woodhead Publishing Ltd. doi:10.1016/0956-7143(94)90030-2.

Hwang, Wook Ryol, and Suresh G. Advani. 2010. "Numerical Simulations of Stokes-Brinkman Equations for Permeability Prediction of Dual Scale Fibrous Porous Media." *Physics of Fluids* 22 (11): 1–15. doi:10.1063/1.3484273.

Jeulin, Dominique, Toufik Kanit, and Samuel Forest. 2004. "Representative Volume Element: A Statistical Point of View." *Continuum Models and Discrete Systems NATO Science Series* 158: 21–27. doi:10.1007/978-1-4020-2316-3.

Jones, Robert M. 1999. *Mechanics of Composite Materials*. 2nd ed. Taylor & Francis.

Kanit, T., S. Forest, I. Galliet, V. Mounoury, and D. Jeulin. 2003. "Determination of the Size of the Representative Volume Element for Random Composites: Statistical and Numerical Approach." *International Journal of Solids and Structures* 40 (13–14): 3647–79. doi:10.1016/S0020-7683(03)00143-4.

Khoun, Lolei, Damien Maillard, and Martin N. Bureau. 2012. "Effect of Process Variables on the Performance of Glass Fibre Composites Made by High Pressure Resin Transfer Moulding."

Lilliefors, Hubert W. 1967. "On the Kolmogorov-Smirnov Test for Normality with Mean and Variance Unknown." *Journal of the American Statistical Association* 62 (318): 399–402.

Lu, K. 2010. "The Future of Metals." *Science* 328 (9): 319–20. doi:10.1016/S0166-2481(08)00028-7.

Lundstrom, T. S., and B. R. Gebart. 1995. "Effect of Perturbation of Fibre Architecture on Permeability Inside Fibre Tows." *Journal of Composite Materials* 29 (4): 424–43. doi:10.1177/002199839502900401.

Massey Jr., Frank J. 1951. "The Kolmogorov-Smirnov Test for Goodness of Fit." *Journal of the American Statistical Association* 46 (253): 68–78. doi:10.1017/CBO9781107415324.004.

Matuzaki, Ryosuke, Daigo Seto, Masaki Naito, Akira Todoroki, and Yoshihiro Mizutani. 2015. "Analytical Prediction of Void Formation in Geometrically Anisotropic Woven Fabrics during Resin Transfer Molding." *COMPOSITES SCIENCE AND TECHNOLOGY* 107. Elsevier Ltd: 154–61. doi:10.1016/j.compscitech.2014.12.013.

Melro, A. R., P. P. Camanho, and S. T. Pinho. 2008. "Generation of Random Distribution of Fibres in Long-Fibre Reinforced Composites." *Composites Science and Technology* 68 (9): 2092–2102. doi:10.1016/j.compscitech.2008.03.013.

Mortensen, Andreas. 2007. *Concise Encyclopedia of Composite Materials*. 2nd ed. Lausanne: Elsevier. doi:10.1017/CBO9781107415324.004.

Nabovati, Aydin, Edward W. Llewellin, and Antonio C M Sousa. 2009. "A General Model for the Permeability of Fibrous Porous Media Based on Fluid Flow Simulations Using the Lattice Boltzmann Method." *Composites Part A: Applied Science and Manufacturing* 40 (6–7). Elsevier Ltd: 860–69. doi:10.1016/j.compositesa.2009.04.009.

Neuman, S. P. 1977. "Theoretical Derivation of Darcy's Law." *Acta Mechanica* 25 (3–4): 153–70. doi:10.1007/BF01376989.

Nixon, J. A. 2000. "Vacuum Infusion: Cost-Effective Closed Mould Processing to Meet the Challenges of the Styrene Issue." In *Integrated Design and Manufacture Using Fibre-*

Reinforced Polymeric Composites, 125–39. Woodhead Publishing Ltd.

Okonkwo, Kenneth. 2010. "3D Permeability Characterization of Fibrous Media." University of Delaware. Msc Thesis

Park, Chung, Aurélie Lebel, Abdelghani Saouab, Joël Bréard, and Woo Lee. 2011. "Modeling and Simulation of Voids and Saturation in Liquid Composite Molding Processes." *Composites Part A* 42 (6). Elsevier Ltd: 658–68. doi:10.1016/j.compositesa.2011.02.005.

Pestana, Maria Helena, and João Nunes Gageiro. 2014. *Análise de Dados Para Ciências Sociais - A Complementaridade Do SPSS*. Edited by Manuel Robalo. 6th ed. Edições Sílabo, Lda.

Pocinho, Margarida, and João Paulo Figueiredo. 2008. *Estatística E Bioestatística*.

Potluri, Prasad, I. Parlak, R. Ramgulam, and T. V. Sagar. 2006. "Analysis of Tow Deformations in Textile Preforms Subjected to Forming Forces." *Composites Science and Technology* 66 (2): 297–305. doi:10.1016/j.compscitech.2005.04.039.

Rudd, C. D., A. C. Long, K. N. Kendall, and C. G. E. Mangin. 1997. *Liquid Moulding Technologies*. 1st ed. Woodhead Publishing Ltd.

Sadiq, T a K, S G Advani, and R S Parnas. 1995. "Experimental Investigation of Transverse Flow-through Aligned Cylinders." *International Journal of Multiphase Flow* 21 (5): 755–74. doi:Doi 10.1016/0301-9322(95)00026-T.

Sanei, Seyed Hamid Reza, and Ray S. Fertig. 2015. "Uncorrelated Volume Element for Stochastic Modeling of Microstructures Based on Local Fiber Volume Fraction Variation." *Composites Science and Technology* 117 (July 2016): 191–98. doi:10.1016/j.compscitech.2015.06.010.

Sangani, A. S., and C. Yao. 1988. "Transport Processes in Random Arrays of Cylinders. II. Viscous Flow." *Physics of Fluids* 31 (9): 2435–44.

Scheidegger, Adrian E. 1974. *The Physics of Flow Through Porous Media*. Edited by University of Toronto Press. 3rd ed.

Shapiro, S S, and M B Wilk. 1965. "An Analysis of Variance Test for Normality (Complete Samples)" 52 (3): 591-. doi:10.2307/2333709.

Šimáček, Pavel, and Suresh G. Advani. 2004. "Desirable Features in Mold Filling Simulations for Liquid Composite Molding Processes." *Polymer Composites* 25 (4): 355–67. doi:10.1002/pc.20029.

Varandas, Luís. 2016. "Micro-Mechanical Modeling of Interlaminar Crack Propagation." Faculdade de Engenharia da Universidade do Porto. MSc Thesis

Vernet, N., E. Ruiz, S. Advani, J. B. Alms, M. Aubert, M. Barburski, B. Barari, et al. 2014. "Experimental Determination of the Permeability of Engineering Textiles: Benchmark II." *Composites Part A: Applied Science and Manufacturing* 61. Elsevier Ltd: 172–84. doi:10.1016/j.compositesa.2014.02.010.

Wilk, M. B., and R. Gnanadesikan. 1968. "Probability Plotting Methods for the Analysis of Data." *Biometrika* 55 (1): 1–17. doi:10.1093/biomet/55.1.1.

Wong, C. C., and A. C. Long. 2006. "Modelling Variation of Textile Fabric Permeability at Mesoscopic Scale." *Plastics, Rubber and Composites* 35 (3): 101–11. doi:10.1179/174328906X103088.

Wongsto, A, and S Li. 2005. "Micromechanical FE Analysis of UD Fibre-Reinforced Composites with Fibres Distributed at Random over the Transverse Cross-Section." *Composites - Part A: Applied Science and Manufacturing* 36: 1246–66. doi:10.1016/j.compositesa.2005.01.010.

Xu, Jian, Stepan Vladimirovitch Lomov, I. Verpoest, S. Daggumati, W. Van Paepegem, and J. Degrieck. 2015. “A Progressive Damage Model of Textile Composites on Meso-Scale Using Finite Element Method: Fatigue Damage Analysis.” *Computers & Structures* 152: 96–112. doi:10.1016/j.compstruc.2015.02.005.

Yazdchi, K., S. Srivastava, and S. Luding. 2011. “On the Validity of the Carman-Kozeny Equation in Random Fibrous Media.” In *II International Conference on Particle-Based Methods*.

Yazdchi, Kazem. 2012. “Micro-Macro Relations for Flow through Fibrous Media.” http://doc.utwente.nl/82288/.

Zhang, F., S. Comas-Cardona, and C. Binetruy. 2012. “Statistical Modeling of in-Plane Permeability of Non-Woven Random Fibrous Reinforcement.” *Composites Science and Technology* 72 (12). Elsevier Ltd: 1368–79. doi:10.1016/j.compscitech.2012.05.008.

Zhu, H. P., Z. Y. Zhou, R. Y. Yang, and A. B. Yu. 2007. “Discrete Particle Simulation of Particulate Systems: Theoretical Developments.” *Chemical Engineering Science* 62 (13): 3378–96. doi:10.1016/j.ces.2006.12.089.

Zhu, H. P., Z. Y. Zhou, R. Y. Yang, and A. B. Yu. 2008. “Discrete Particle Simulation of Particulate Systems: A Review of Major Applications and Findings.” *Chemical Engineering Science* 63 (23): 5728–70. doi:10.1016/j.ces.2008.08.006.

Appendix A: Matlab® Script for analysis automation - "Analysis_coordinator" module

Appendix A contains the code of the Matlab® script "Analysis_coordinator". This module is responsible to handle the analysis inputs, as explained in Chapter 3.

```
%----------------------------------------
%----INPUT VARIABLES---------------------
%Array of RVE sizes
RVEsizerange=[6,8,10,12,16,20,24];
%Array of Fibre Volume Fractions
Vfrange=[0.5,0.55,0.6,0.65,0.7,0.75,0.78];
%Number of samples per RVE size or Vf
iterationnumber=145;
%----------------------------------------


%-------------------------------------------------------------------
%----DECIDE WETHER THE ANALYSIS IS MADE FOR Vf(0) or RVE SIZE(1)----
decision=0;
%-------------------------------------------------------------------


if decision==1;
    analysisvariable=RVEsizerange;
elseif decision==0
    analysisvariable=Vfrange;
end

%--CREATE WORK DIRECTORY---
if exist('C:\Temp')==0
    mkdir('C:\Temp');
end

mkdir('C:\Temp\PermeabilityAnalysis');
mkdir('C:\Temp\PermeabilityAnalysis\AnalysisINP');
mkdir('C:\Temp\PermeabilityAnalysis\TemporaryResults');
addpath(genpath('C:\Temp'))



dlmwrite('C:\Temp\iteration_number.txt',iterationnumber);
savevariables(1,:)=RVEsizerange;
savevariables(2,:)=Vfrange;
savevariables(3,:)=analysisvariable;
dlmwrite('C:\Temp\Coordinator_variables.txt',savevariables);


for nbm=5:length(analysisvariable)
    analysisvalue=analysisvariable(1,nbm);
    Analysis_iterator;
    savevariables=dlmread('C:\Temp\Coordinator_variables.txt');
    RVEsizerange=savevariables(1,:);
    Vfrange=savevariables(2,:);
    analysisvariable=savevariables(3,:);
end

disp('Done!')
```

Appendix B: Matlab® Script for analysis automation - "Analysis_iterator" module

Appendix B contains the code of the "Analysis_iterator" module, responsible to handle the iterative cycles described in Chapter 3.

```
%WORK DIRECTORY INFORMATION
parentdirectory='C:\Temp\PermeabilityAnalysis';
analysisdirectory='C:\Temp\PermeabilityAnalysis\AnalysisINP';
temporaryresults='C:\Temp\PermeabilityAnalysis\TemporaryResults';


if decision==0
    RVEVf=analysisvalue;
    RVEsize=12;
    mkdir(strcat(parentdirectory,'\',num2str(RVEVf)))
elseif decision==1
    RVEVf=0.7;
    RVEsize=analysisvalue;
    mkdir(strcat(parentdirectory,'\',num2str(RVEsize)))
end


%ANSYS FLUENT RUN COMMAND
runfluent=strcat('C:\"Program Files"\"ANSYS
Inc"\v170\fluent\ntbin\win64\fluent.exe 3ddp -g -wait -i
C:\Temp\AnalysisJournal',num2str(RVEsize),'.txt');



savevariables2={parentdirectory;analysisdirectory;temporaryresults;runfluen
t};
fileID=fopen('C:\Temp\Iterator_variables.txt','w');
for nrow=1:length(savevariables2)
    formatSpec = '%s\n';
    fprintf(fileID,formatSpec,savevariables2{nrow,:});
end
fclose(fileID);
savevariables3=[RVEVf;RVEsize;decision];
dlmwrite('C:\Temp\Iterator_variables2.txt',savevariables3);



%ITERATIVE CYCLE

z=1;
while z<=iterationnumber
    dlmwrite('iteno.txt',z);
    2D_RVE_generator;
    !cd C:\Temp && abaqus cae noGUI=matlababaqus_3D.py
    while exist('Job-1.inp')==0
        pause(2);
        disp('pausing')
    end
    movefile('C:\Temp\Job-1.inp',strcat(analysisdirectory,'\Job.inp'));

delete(strcat(temporaryresults,'\INLET'),strcat(temporaryresults,'\OUTLET')
,strcat(temporaryresults,'\fluxes.txt'),strcat(temporaryresults,'\velocity.
txt'));
```

```
    for planedeletion=0:8
        delete(strcat(temporaryresults,'\PLANE',num2str(planedeletion)));
    end
    dos(runfluent);
    disp('waiting for simulation results')
    if exist(strcat(temporaryresults,'\velocity.txt'))==0
        dlmwrite('iteration_number.txt',iterationnumber);
        clear all
        iterationnumber=dlmread('iteration_number.txt');
        savevariables3=dlmread('C:\Temp\Iterator_variables2.txt');
        RVEsize=savevariables3(2,1);
        RVEVf=savevariables3(1,1);
        decision=savevariables3(3,1);
        savevariables2=importdata('C:\Temp\Iterator_variables.txt');
        parentdirectory=savevariables2{1,1};
        analysisdirectory=savevariables2{2,1};
        temporaryresults=savevariables2{3,1};
        runfluent=savevariables2{4,1};
        z=dlmread('iteno.txt');
        iterationnumber=dlmread('iteration_number.txt');
    else
        Permeability_calculator;

delete(strcat(temporaryresults,'\INLET'),strcat(temporaryresults,'\OUTLET')
,strcat(temporaryresults,'\fluxes.txt'),strcat(temporaryresults,'\velocity.
txt'));
        for planedeletion=0:8

delete(strcat(temporaryresults,'\PLANE',num2str(planedeletion)));
        end
        z=z+1;
        dlmwrite('iteno.txt',z);
        clear all
        iterationnumber=dlmread('iteration_number.txt');
        savevariables3=dlmread('C:\Temp\Iterator_variables2.txt');
        RVEsize=savevariables3(2,1);
        RVEVf=savevariables3(1,1);
        decision=savevariables3(3,1);
        savevariables2=importdata('C:\Temp\Iterator_variables.txt');
        parentdirectory=savevariables2{1,1};
        analysisdirectory=savevariables2{2,1};
        temporaryresults=savevariables2{3,1};
        runfluent=savevariables2{4,1};
        z=dlmread('iteno.txt');
        iterationnumber=dlmread('iteration_number.txt');
    end
end
```

Appendix C: Matlab® Script for analysis automation - "Permeability_calculator" module

Appendix C contains the code of the "Permeability_calculator" module, responsible to calculate permeability values, as well as export them to text files (.txt) in each iterative cycle of the "Analysis_iterator" module.

```
%---NET-FLUX IMBALANCE CONTROL---
fluxdata=importdata(strcat(temporaryresults,'\fluxes.txt'));
fluxdata=fluxdata.data;
fluximbalance=(fluxdata(1,1)-abs(fluxdata(2,1)))/fluxdata(1,1);
if fluximbalance<0.01


    if decision==0
        savedirectory=strcat(parentdirectory,'\',num2str(RVEVf));
    elseif decicion==1
        savedirectory=strcat(parentdirectory,'\',num2str(RVEsize));
    end



    %number of interior planes (starts in 0) -- DO NOT CHANGE
    planenumber=8;



    %------ CALCULATING AVERAGE PRESSURE VALUES ON BOUNDARY CONDITIONS ----
    pause(1);
    ipfile=strcat(temporaryresults,'\INLET');
    ipdata=importdata(ipfile);

    irawdata=ipdata.data;
    ipressuredata=irawdata(:,5);


    IPnumlines=size(ipressuredata);
    IPnumlines=IPnumlines(1,1);

    aveIP=sum(ipressuredata)/IPnumlines;

    pause(1);
    %------BOUNDARY PLANES AVERAGE PRESSURE AQUISITION------
    opfile=strcat(temporaryresults,'\OUTLET');
    opdata=importdata(opfile);

    orawdata=opdata.data;
    opressuredata=orawdata(:,5);

    OPnumlines=size(opressuredata);
    OPnumlines=OPnumlines(1,1);

    aveOP=sum(opressuredata)/OPnumlines;

    %-------- CALCULATE AVERAGE PRESSURE VALUES ON INTERIOR PLANES --------
    for ztp=0:planenumber
        planefile=strcat(temporaryresults,'\PLANE',num2str(ztp));
        planedata=importdata(planefile);
```

```
        planedata=planedata.data;
        planepressure=planedata(:,5);
        planenumlines=size(planepressure);
        planenumlines=planenumlines(1,1);
        aveplanepressure=sum(planepressure)/planenumlines;
        InPlanePressure(ztp+1,1)=aveplanepressure;
    end

    %-------- CALCULATE TOTAL GLOBAL PERMEABILITY ON THE RVE --------------

    Vf=0.7;
    length=RVEsize*(4e-6);
    rho=889;
    niu=1.06;

    vfile=strcat(temporaryresults,'\velocity.txt');
    Vel=importdata(vfile);
    v=Vel.data;

    dpdx=(aveIP-aveOP)/length;
    permeability=(v/dpdx)*niu;


    %----- CALCULATE PERMEABILITY IN INTERIOR PLANES --------------

    for w=0:planenumber-1
        dpdx(w+1)=(InPlanePressure(w+1,1)-
InPlanePressure(w+2,1))/(length/4);
        K(w+1,1)=(v/dpdx(1,w+1))*niu;
    end

    dpdxi0=(aveIP-InPlanePressure(1,1))/(length/4);
    Ki0=(v/dpdxi0)*niu;
    dpdx2o=(InPlanePressure(planenumber+1,1)-aveOP)/(length/4);
    K2o=(v/dpdx2o)*niu;


    %------ EXPORT PERMEABILITY RESULTS --------------
    permvariablenames={'Total
permeability';'Ki0';'K01';'K12';'K23';'K34';'K45';'K56';'K67';'K78';'K8o'};
    permValues=[permeability;Ki0;K;K2o];
    permeabilityTable=table(permValues,'RowNames',permvariablenames);


writetable(permeabilityTable,strcat(savedirectory,'\',num2str(z),'permeabil
ity.txt'));

    %------- EXPORT PRESSURE RESULTS ---------------

pressurevariablenames={'Pin';'P0';'P1';'P2';'P3';'P4';'P5';'P6';'P7';'P8';'
Pout'};
    pressureValues=[aveIP;InPlanePressure;aveOP];
    pressureTable=table(pressureValues,'RowNames',pressurevariablenames);


writetable(pressureTable,strcat(savedirectory,'\',num2str(z),'pressure.txt'
));

else
    disp('Error in numerical simulation')
end
```

Appendix D: Journal File for CFD simulation in ANSYS Fluent®

Appendix D contains an example of a journal file responsible to conduct the CDF simulation in ANSYS Fluent® for an RVE size N_f=12.

```
(set! *cx-exit-on-error* #t)
/file/import/abaqus input C:\Temp\PermeabilityAnalysis\AnalysisINP\Job.inp
/mesh scale 1e-6 1e-6 1e-6
/define/models/viscous laminar yes
/define/materials copy fluid engine-oil
/define/boundary-conditions/modify-zones zone-type solid-7 fluid
/define/boundary-conditions fluid solid-7 yes engine-oil no no no no 0 no 0 no 0 no
0 no 0 no 1 no no no no
/define/boundary-conditions zone-type assembly.matrix-1.left interface
/define/boundary-conditions zone-type assembly.matrix-1.right interface
/define/boundary-conditions zone-type assembly.matrix-1.upper interface
/define/boundary-conditions zone-type assembly.matrix-1.down interface
/define/boundary-conditions zone-type assembly.matrix-1.inlet velocity-inlet
/define/boundary-conditions zone-type assembly.matrix-1.outlet outflow
/define/boundary-conditions velocity-inlet assembly.matrix-1.inlet no yes yes no 0
yes no 0 no 0 no 0.01
/define/boundary-conditions outflow assembly.matrix-1.outlet 1
/define/mesh-interfaces make-periodic assembly.matrix-1.left assembly.matrix-
1.right no , , , yes no l-r
/define/mesh-interfaces make-periodic assembly.matrix-1.upper assembly.matrix-
1.down no , , , yes no u-d
/report/reference-values velocity 0.01
/solve/initialize/set-defaults pressure 0
/solve/initialize/set-defaults x-velocity 0
/solve/initialize/set-defaults y-velocity 0
/solve/initialize/set-defaults z-velocity 0.01
/solve/initialize initialize-flow
/solve iterate 200
/report/fluxes mass-flow no assembly.matrix-1.inlet assembly.matrix-1.outlet () yes
C:\Temp\PermeabilityAnalysis\TemporaryResults\fluxes.txt
/report/volume-integrals volume-avg solid-7 () z-velocity yes
C:\Temp\PermeabilityAnalysis\TemporaryResults\velocity.txt
/surface plane-surf-aligned plane0 assembly.matrix-1.inlet 0 0 4.8e-6
/surface plane-surf-aligned plane1 assembly.matrix-1.inlet 0 0 9.6e-6
/surface plane-surf-aligned plane2 assembly.matrix-1.inlet 0 0 1.44e-5
/surface plane-surf-aligned plane3 assembly.matrix-1.inlet 0 0 1.92e-5
/surface plane-surf-aligned plane4 assembly.matrix-1.inlet 0 0 2.4e-5
```

```
/surface plane-surf-aligned plane5 assembly.matrix-1.inlet 0 0 2.88e-5

/surface plane-surf-aligned plane6 assembly.matrix-1.inlet 0 0 3.36e-5

/surface plane-surf-aligned plane7 assembly.matrix-1.inlet 0 0 3.84e-5

/surface plane-surf-aligned plane8 assembly.matrix-1.inlet 0 0 4.32e-5

/file/export ascii C:\Temp\PermeabilityAnalysis\TemporaryResults\INLET
assembly.matrix-1.inlet () yes pressure () no

/file/export ascii C:\Temp\PermeabilityAnalysis\TemporaryResults\OUTLET
assembly.matrix-1.outlet () yes pressure () no

/file/export ascii C:\Temp\PermeabilityAnalysis\TemporaryResults\PLANE0 plane0 ()
yes pressure () no

/file/export ascii C:\Temp\PermeabilityAnalysis\TemporaryResults\PLANE1 plane1 ()
yes pressure () no

/file/export ascii C:\Temp\PermeabilityAnalysis\TemporaryResults\PLANE2 plane2 ()
yes pressure () no

/file/export ascii C:\Temp\PermeabilityAnalysis\TemporaryResults\PLANE3 plane3 ()
yes pressure () no

/file/export ascii C:\Temp\PermeabilityAnalysis\TemporaryResults\PLANE4 plane4 ()
yes pressure () no

/file/export ascii C:\Temp\PermeabilityAnalysis\TemporaryResults\PLANE5 plane5 ()
yes pressure () no

/file/export ascii C:\Temp\PermeabilityAnalysis\TemporaryResults\PLANE6 plane6 ()
yes pressure () no

/file/export ascii C:\Temp\PermeabilityAnalysis\TemporaryResults\PLANE7 plane7 ()
yes pressure () no

/file/export ascii C:\Temp\PermeabilityAnalysis\TemporaryResults\PLANE8 plane8 ()
yes pressure () no

/exit ok
```